

## Large and small field inflation from hyperbolic sigma models

Rolf Schimmrigk <sup>\*</sup>

*Department of Physics, Indiana University at South Bend, 1700 Mishawaka Avenue, South Bend, Indiana 46634, USA*

 (Received 23 August 2021; accepted 15 February 2022; published 30 March 2022)

Long standing themes in inflation include the issue of large field vs. small field inflation as well as the question what fraction of phase space leads to sufficient inflation and furthermore is compatible with the experimental data. In the present paper, these issues are discussed in the context of modular inflation, a specialization of the framework of automorphic nonlinear  $\sigma$  models associated to homogeneous spaces  $G/K$  in which the continuous shift symmetry group  $G$  is weakly broken to discrete subgroups  $\Gamma$ . The target spaces of these theories inherit a curved structure from the group  $G$ , which in the case of modular invariant inflation leads to a hyperbolic field space geometry. It is shown that in this class of models the symmetry structure leads to both large and small field inflationary trajectories within a single modular inflation model. The present paper analyzes the concrete model of  $j$ -inflation, a hyperbolic model with nontrivial inflaton interactions. It describes in some detail the structure of the initial conditions, including a systematic analysis of several phenomenological functions on the target space, leading to constraints on the curvature scalar of the field space by upcoming experiments, as well as a discussion of the scaling behavior of the spectral index, the finite volume fraction of the field space leading to sufficient inflation, the attractor behavior of  $j$ -inflation, and a comparison of inflaton trajectories vs. target space geodesics. The tensor-ratio analysis shows that  $j$ -inflation is an interesting target for upcoming ground and satellite experiments.

DOI: [10.1103/PhysRevD.105.063541](https://doi.org/10.1103/PhysRevD.105.063541)

### I. INTRODUCTION

The cosmic microwave background (CMB) experiments that have been conducted over the past decade have led to dramatic constraints on the parameters of the models that make up the extensive landscape of the inflationary theory space [1–3]. While most of the progress has come from satellite probes, such experiments are currently continued on the ground in several observatories around the globe, the results of which will provide further insight into the theoretical parameter space [4–6]. While the observables measured or bounded by these experiments provide constraints strong enough to exclude whole classes of models at high confidence levels, the surviving theory space remains large and unstructured. The amorphous nature of this space can be ameliorated somewhat by the introduction of symmetry groups into multifield inflation that are motivated by the fact that they provide an embedding of the shift symmetry. Shift symmetries are often introduced as an *ad hoc* device to ensure the absence of terms that otherwise might affect the small parameters that enter the

observables of the theory. Embedding these symmetries into a proper discrete group has the benefit of allowing a quantitative characterization of the model space by leading to a foliation structure.

In the framework of automorphic inflation, the groups that contain the shift symmetry arise from nonlinear sigma models associated to homogeneous spaces  $G/K$  constructed from reductive groups  $G$  and maximal compact subgroups  $K$ . The resulting field space is curved with a target space metric that is determined by the group  $G$  [7,8]. The discrete groups are obtained from potentials that weakly break the continuous symmetry group  $G(\mathbb{R})$  to subgroups  $\Gamma \subset G(\mathbb{Z})$  defined over integers  $\mathbb{Z}$ . In the simplest case of modular inflation, the discrete shift symmetry results from the weak breaking of the continuous Möbius group  $SL(2, \mathbb{R})$  to congruence subgroups  $\Gamma$  of the modular group  $SL(2, \mathbb{Z})$ . This approach was introduced for the case of level one modularity in [9,10] and for higher level in [11]. The field space of modular inflation carries a nontrivial hyperbolic geometry that derives from the homogeneous space  $G/K = SL(2, \mathbb{R})/SO(2, \mathbb{R})$ , and it was shown in [9] that this metric has important implications for the theory in that the geometry induces new terms in the observables, as compared to a flat theory, that makes these observables quasimodular, thereby preserving the modularity but not the underlying holomorphic nature. This resolves a general issue of modular invariant inflation that was left open in earlier work in the particular context of

<sup>\*</sup>rschimmr@iu.edu

*Published by the American Physical Society under the terms of the Creative Commons Attribution 4.0 International license. Further distribution of this work must maintain attribution to the author(s) and the published article's title, journal citation, and DOI. Funded by SCOAP<sup>3</sup>.*

supergravity. The idea to embed the shift symmetry into the modular group and to focus on the hyperbolic geometry that was emphasized after the appearance of [7] also in the papers [12,13]. Recent discussions concerned with the shift symmetry include [14,15].

The concrete models briefly explored in earlier work include the model of  $j$ -inflation at modular level one [7,9] and the model of  $h_2$ -inflation at level two [11]. It was shown in these papers that these models admit inflaton trajectories that are compatible with the PLANCK data. The compatibility of  $j$ -inflation with experiments thus represents the first hyperbolic two field inflation model consistent with the current cosmological data. Work prior to [7] based on hyperbolic field space aimed at models with single field potentials or effectively single field trajectories, for example, [16,17]. Subsequent work with a focus on inflaton orbits often adopted isomorphic versions such as the Poincaré disk or the Beltrami-Klein models. This includes, for example, Refs. [18,19] and [20–28]. Inflationary models based on negatively curved target spaces have also been considered in other recent work [14,29–34] and have played a role in the discussion of the conjectures concerned with the swampland [11,26,35].

The goal of the present paper is to give a systematic analysis of modular inflation by considering in some detail the slow-roll phase space of  $j$ -inflation, relevant for the observable CMB regime. This analysis leads to a number of observations that are of relevance beyond the specific model considered here. One of these concerns is the issue of large and small field inflation. The distinction between inflaton fields with values larger or smaller than the Planck mass has been a recurrent theme and has often been used as a classification scheme to characterize different types of inflationary models. In modular inflation, it is possible to decompose the field space into separate regions, the union of which gives the total target space. The structures that appear in these separate regions are then repeated infinitely many times in the field space. The nontrivial hyperbolic geometry of these individual regions is given by the metric considered originally by Liouville, Riemann, Beltrami, and Klein, hence is naturally called the Poincaré metric in the literature. This metric leads to a stretching of the field space as one approaches the boundary of the space, in particular, when approaching the origin of the space. This leads to trajectories with initial values that can approach the origin arbitrarily close, thus leading to initial field values that become small at any scale, in particular, compared to the Planck mass. Far away from the origin, one or both of the inflaton components can be large, leading to large field inflation. This shows that in modular inflation, and more generally in the context of curved field space inflation, both small and large field inflation can be realized in the same model.

Modular inflation is a field theory framework with curved target space geometry; hence, it is of interest to ask whether the dynamics of the theory imposes constraints

that lead to deviations from the geodesic structure induced by the metric. It will be shown that while in  $j$ -inflation *per se* the inflaton trajectories are strongly affected by the potential, they also show attractor behavior in the sense that there are certain basins in the target space to which the trajectories converge.

After the discussion of the modular symmetry and the comparison of  $j$ -inflation trajectories with hyperbolic geodesics, the first phenomenological focus of the present exploration is to identify those regions of the target space that lead to inflation with a number of  $e$ -folds in some standard range. This first step is similar in spirit to earlier investigations of other inflationary models such as hybrid inflation (see, e.g., [36–45]) and other models [46], which focused on the question of the existence of inflation *per se*, implemented as a lower bound on the number of  $e$ -folds. In the context of considering the global scale structure of the field space, it is of interest that in modular inflation the target space comes equipped with a finite measure that allows to quantify the volume in phase space that leads to inflation. This is possible without the need of a regularization of this measure, an issue that has afflicted many discussions in this context [47–52].

In the context of sufficient inflation, the spectral index and the tensor ratio are left unconstrained. The data obtained by extending the analysis to these parameters can be used to address a question that concerns the possible scaling of the spectral index and the tensor ratio. This was explored for single field inflation in several papers [53–55], with the aim of providing *a priori* constraints in the plane spanned by these two parameters. The important question is what the behavior is of these two parameters in multifield inflation. Finally, given the experimental data obtained from the CMB satellites, it is of interest to consider how these observational results constrain the regions of viable initial conditions beyond those obtained by the  $e$ -fold constraint alone.

The outline of this paper is as follows. In Secs. II and III, multifield inflation and modular inflation are briefly reviewed to establish the general context and the notation used here. Section IV describes the global structure of the potential of  $j$ -inflation. Section V discusses the modular structure of the critical points on the potential surface and explains the associated existence of both large field and small field inflation in the framework of modular invariant sigma models. Section VI shows that in the global target space there are broad basins of attraction and compares the resulting inflaton trajectories with the geodesics of the hyperbolic geometry. Section VII analyzes the behavior of the  $e$ -fold function  $N_*$  on the target space and shows that a finite volume fraction of the target space leads to sufficient inflation, where the volume is obtained from the nontrivial geometric measure on the field space. Sections VIII and IX consider the spectral index as a function on the target space, including a discussion of the scaling behavior of the spectral index. Section X analyzes the behavior of the

tensor-to-scalar ratio on the field space. It is shown how the bounds on  $r$  provided by the CMB probes constrain the curvature scalar of the field space and that  $j$ -inflation presents an interesting target for the upcoming CMB experiments such as the Simons Observatory, as well as LightBird and CMB-S4. This leads to a discussion of large field inflation vs. small values of the tensor ratio, as well as of the swampland conjectures. Section XI analyzes how the variation of the mass scale of  $j$ -inflation impacts the constraints of the CMB on the model. Section XII presents the conclusions.

## II. FORMULATION OF GENERAL MULTIFIELD INFLATION

Automorphic inflation is a multifield inflation framework with fields  $\phi^I, I = 1, \dots, n$  and a target space metric  $G_{IJ}(\phi^K)$  that leads to a nontrivial kinetic coupling action,

$$\mathcal{A} = - \int d^4x \sqrt{-g} \left( \frac{1}{2} G_{IJ}(\phi^K) g^{\mu\nu} \partial_\mu \phi^I \partial_\nu \phi^J + V(\phi^I) \right). \quad (1)$$

The perturbations relevant in this general context can be parametrized as  $(\mathcal{R}, S^{IJ})$ , where  $\mathcal{R}$  is the comoving curvature perturbation of Lukash and Bardeen [56,57] (see also [58]),

$$\mathcal{R} = H\delta u - \psi, \quad (2)$$

formulated in terms of the spacetime metric perturbation  $\psi$  and  $\delta u$ , obtained from the divergence part of the energy-momentum tensor perturbation  $\delta T_{0i}$  (see [9] for details), and  $S^{IJ}$  is the tensor of isocurvature perturbations [9],

$$S^{IJ} = \frac{H}{\dot{\sigma}} (\sigma^I Q^J - \sigma^J Q^I). \quad (3)$$

Here  $H = \dot{a}/a$  is the Hubble-Slipher parameter,  $\dot{\sigma} = (G_{IJ} \dot{\phi}^I \dot{\phi}^J)^{1/2}$  is the speed of the background inflaton, and  $\sigma^I = \dot{\phi}^I / \dot{\sigma}$  is the normalized inflaton velocity. The closed form of the large scale dynamics of the system  $(\mathcal{R}, S^{IJ})$  was derived in [9] as

$$\begin{aligned} \dot{\mathcal{R}} &= -2H\eta_{IK}\sigma^K\sigma^J S^{IJ}, \\ D_i S^{IJ} &= 2H(\eta_{KL}\sigma^K\sigma^L - \epsilon)S^{IJ}, \\ &+ H \left( \eta_{KL} G^{K[I} S^{J]L} - \frac{\epsilon}{3} M_{\text{Pl}}^2 \sigma^{[I} R^J]_{KLM} \sigma^K S^{LM} \right), \end{aligned} \quad (4)$$

where  $\epsilon = -\dot{H}/H^2$  is the slow-roll parameter,

$$\eta_{IJ} = M_{\text{Pl}}^2 \frac{V_{;IJ}}{V}, \quad (5)$$

and  $V^{[I} W^{J]} = V^I W^J - V^J W^I$ . The covariant derivative  $D_i$  acts on the contravariant tensor  $S^{IJ}$ . A more detailed

discussion and the specialization to the two field case  $(\mathcal{R}, \mathcal{S})$  can be found in [9].

The parameters considered in the present analysis include the spectral index  $n_{\mathcal{R}\mathcal{R}}$  of the scalar power spectrum  $\mathcal{P}_{\mathcal{R}\mathcal{R}}$  of  $\mathcal{R}$ , the tensor ratio, and the number of  $e$ -folds,

$$\begin{aligned} \mathcal{P}_{\mathcal{R}\mathcal{R}} &= A_{\mathcal{R}\mathcal{R}} \left( \frac{k}{k_*} \right)^{n_{\mathcal{R}\mathcal{R}}-1}, & \mathcal{P}_T &= A_T \left( \frac{k}{k_*} \right)^{n_T}, \\ r &= \frac{\mathcal{P}_T}{\mathcal{P}_{\mathcal{R}\mathcal{R}}}, & N_* &= \int_{t_*}^{t_e} H dt. \end{aligned} \quad (6)$$

The general expressions in multifield inflation with an inflaton multiplet  $\phi^I$  and a curved target space metric  $G_{IJ}$  are given by

$$\begin{aligned} n_{\mathcal{R}\mathcal{R}} &= 1 - 3G^{IJ}\epsilon_I\epsilon_J + 2\frac{\eta_{IJ}\epsilon^I\epsilon^J}{G^{KL}\epsilon_K\epsilon_L}, \\ r &= 8G^{IJ}\epsilon_I\epsilon_J, \\ n_T &= -\frac{r}{8}, \end{aligned} \quad (7)$$

where the slow-roll parameters  $\epsilon_I$  are defined as

$$\epsilon_I = M_{\text{Pl}} \frac{V_{;I}}{V}. \quad (8)$$

The slow-roll dynamics can be written in terms of the potential as

$$\dot{\phi}^I = -\sqrt{\frac{V}{3}} G^{IJ} \epsilon_J. \quad (9)$$

A systematic analysis of models in such a framework involves in the first instance the variation of the energy scales that define the model, as well as a scan of the phase space of the theory. In the context of the phase space analysis, the question of a measure arises, a problem that involves the geometry of the target space. Other questions include the dichotomy of large vs. small field inflation, an issue that also turns out to depend on the geometry of the field space. Finally, one can ask whether the scaling behavior of the CMB observables observed in simple single field models has some counter part in the multifield context.

## III. STRUCTURE OF MODULAR INFLATION ON HYPERBOLIC FIELD SPACE

This section briefly outlines the essential structures that are used in the remainder of this paper. Modular inflation is a framework of two field inflation that specializes the multifield theory of automorphic inflation [7,8]. The latter is based on automorphic functions  $F(\phi^I)$ , where the inflaton multiplet defines the coordinates of quotient spaces  $G/K$ , defined in terms of reductive groups  $G$  and maximal compact subgroups  $K$ .

In the simplest case, the doublet spans the curved target space geometry given by the upper half plane  $\mathcal{H}$ , which can be identified as the homogeneous space,

$$\mathcal{H} := \mathrm{SL}(2, \mathbb{R})/\mathrm{SO}(2, \mathbb{R}). \quad (10)$$

The geometry of this space is determined by the hyperbolic metric,

$$G_{IJ} := \frac{\mu^2}{(\phi^2)^2} \delta_{IJ}, \quad I, J = 1, 2, \quad (11)$$

where  $\mu$  is an *a priori* arbitrary energy scale. This metric of the upper half plane leads to a space of constant curvature,

$$R = -\frac{2}{\mu^2}. \quad (12)$$

Hence, the energy scale  $\mu$  can be thought of as a measure of the curvature of the target space. In distinction to the energy scale  $\Lambda$ , the parameter  $\mu$  enters all the formulas that characterize  $j$ -inflation. As a result, the analyses below show that the curvature scalar  $R$  is constrained by the CMB experiments. The hyperbolic modular inflation metric admits an isometry group that contains the Möbius group and the transformation  $\tau \mapsto (-\bar{\tau})$ .

In modular inflation, it is convenient to complexify the inflaton doublet as  $\phi = \phi^1 + i\phi^2$  and to introduce the dimensionless inflaton as  $\tau = \phi/\mu$ . This recovers the so-called Poincaré metric of Liouville, Beltrami, and Klein as  $ds^2 = \mu^2 d\tau d\bar{\tau}/(\mathrm{Im}\tau)^2$ . An important feature of hyperbolic geometry is that, while the curvature is constant, the metric diverges as it approaches the boundary of the space  $\phi^2 = 0$ ; hence, the target space in this parametrization is the upper half plane  $\phi^2 > 0$ . The form of the boundary can be transformed into different shapes if different variables are used, such as in the Poincaré disk model which is obtained via the Cayley transform and which was considered later in [12,13]. Other models include the sinh form of the metric considered more recently in [20,23,27,31]. These related models of the hyperbolic geometry can be described in terms of homogeneous spaces based on quotients of the groups  $\mathrm{SU}(1, 1)$  and  $\mathrm{SO}(2, 1)$  instead of  $\mathrm{SL}(2, \mathbb{R})$ . This setup can be compared to the metric sometimes considered in axion-dilaton inflation with a radial field  $\rho$  and an angular field  $\theta$  with a semiflat metric that depends on the radial field only. Writing the complex field as  $\phi = \rho e^{i\theta}$  leads to the modular inflation metric  $G_{IJ} = \mu^2 \delta_{IJ}/\rho^2 \sin^2 \theta$  involving both target space directions.

Given a hyperbolic metric on the target space with an associated symmetry group, it is natural to consider potentials that preserve at least some of these symmetries. In modular inflation, the idea is to break the continuous Möbius group  $\mathrm{SL}(2, \mathbb{R})$  to an infinite discrete group  $\Gamma$  of the modular group  $\mathrm{SL}(2, \mathbb{Z})$  that contains the shift symmetry,

$$\mathrm{SL}(2, \mathbb{R}) \xrightarrow{V_\Gamma} \Gamma \subset \mathrm{SL}(2, \mathbb{Z}), \quad (13)$$

where the potential

$$V_\Gamma = \Lambda^4 |F|^2 \quad (14)$$

is defined in terms of a function  $F$  that is constructed from modular forms in such a way as to be invariant under the group  $\Gamma$ . This allows for nontrivial potentials in which both components of the inflaton doublet are coupled in a nontrivial way. In the present paper, the focus is on the full modular group  $\Gamma = \mathrm{SL}(2, \mathbb{Z})$ , in which case modular invariant inflation potentials can be constructed in terms of the Eisenstein series modular forms  $E_4, E_6$ , of weight four and six, respectively, which are defined as

$$E_w(\tau) = 1 - \frac{2w}{B_w} \sum_{n \geq 1} \sigma_{w-1}(n) q^n, \quad (15)$$

where  $q = e^{2\pi i \tau}$ , the denominators  $B_w$  are the Bernoulli numbers, and  $\sigma_w(n)$  is the divisor function [7,9].

In general modular inflation, the models involve a modular invariant function  $F(\phi^1/\mu)$ , hence depend in the formulation given here on the energy scale  $\mu$  that enters the potential. As a result, the slow-roll parameters  $\epsilon_I$  depend on  $\mu$  and can be expressed in the form [9]

$$\epsilon_I = i^{I-1} \frac{M_{\mathrm{Pl}}}{\mu} \left( \frac{F'}{F} + (-1)^{I-1} \frac{\bar{F}'}{\bar{F}} \right), \quad (16)$$

leading to

$$\epsilon_V = \frac{1}{2} G^{IJ} \epsilon_I \epsilon_J = 2 \frac{M_{\mathrm{Pl}}^2}{\mu^2} (\mathrm{Im}\tau)^2 \left| \frac{F'}{F} \right|^2. \quad (17)$$

The cosmological parameters considered above can be shown to be expressed in a quasimodular form via

$$K_F = \left[ 2 \left| \frac{F'}{F} \right|^2 - \mathrm{Re} \left( \frac{F'' \bar{F}'}{F' \bar{F}} \right)_{\mathrm{mod}} + \frac{\pi}{3} \mathrm{Im} \left( \hat{E}_2 \frac{\bar{F}'}{\bar{F}} \right) \right] \quad (18)$$

as [9]

$$\begin{aligned} n_{\mathcal{R}\mathcal{R}} &= 1 - 4 \frac{M_{\mathrm{Pl}}^2}{\mu^2} (\mathrm{Im}\tau)^2 K_F, \\ r &= 32 \frac{M_{\mathrm{Pl}}^2}{\mu^2} (\mathrm{Im}\tau)^2 \left| \frac{F'}{F} \right|^2, \\ N_* &= \frac{1}{\sqrt{3}} \frac{\Lambda^2}{M_{\mathrm{Pl}}} \int_{t_*}^{t_e} dt |F(\tau(t))|, \end{aligned} \quad (19)$$

where the quasimodular form  $\hat{E}_2$  is defined as

$$\hat{E}_2(\tau) = E_2(\tau) - \frac{3}{\pi(\text{Im } \tau)}. \quad (20)$$

This shows that the spectral index is a modular invariant quantity, an issue that was not addressed in the earlier literature, for example, in the context of supergravity theories.

The model of  $j$ -inflation is defined at level  $N = 1$ ; i.e., it is invariant under the full modular group  $\text{SL}(2, \mathbb{Z})$  with  $F(\tau) = j(\tau)$ . This group  $\text{SL}(2, \mathbb{Z})$  contains the shift symmetry of the inflaton. The  $j$  function is most naturally defined as the quotient of two modular forms of weight 12,

$$j(\tau) := \frac{E_4^3(\tau)}{\Delta(\tau)}, \quad (21)$$

where  $\Delta(\tau) = \eta^{24}(\tau)$  is the Ramanujan modular cusp form of the full modular group, expressed in terms of the Dedekind eta function,

$$\eta(\tau) = q^{1/24} \prod_{n \geq 1} (1 - q^n). \quad (22)$$

The Ramanujan form can be written in terms of the generators  $E_4, E_6$  of the space of all modular forms relative to the modular group  $\text{SL}(2, \mathbb{Z})$  as  $\Delta = (E_4^3 - E_6^2)/1728$ .

The slow-roll parameters  $\epsilon_I$  can now be expressed directly in terms of undifferentiated modular forms as

$$\epsilon_I = -2\pi i^I \frac{M_{\text{Pl}}}{\mu} \left( \frac{E_6}{E_4} + (-1)^I \frac{\bar{E}_6}{\bar{E}_4} \right), \quad (23)$$

with

$$\epsilon_V = 8\pi^2 \frac{M_{\text{Pl}}^2}{\mu^2} (\text{Im } \tau)^2 \left| \frac{E_6}{E_4} \right|^2, \quad (24)$$

and the above parameters are given directly in terms of the Eisenstein series via

$$K_j = \left[ 8 \left| \frac{E_6}{E_4} \right|^2 - 3 \text{Re} \left( \frac{E_4^2 \bar{E}_6}{E_6 \bar{E}_4} \right) + \text{Re} \left( \hat{E}_2 \frac{\bar{E}_6}{\bar{E}_4} \right) \right], \quad (25)$$

as [7,8]

$$\begin{aligned} n_{\mathcal{R}\mathcal{R}} &= 1 - \frac{8\pi^2 M_{\text{Pl}}^2}{3 \mu^2} (\text{Im } \tau)^2 K_j, \\ r &= 128\pi^2 \frac{M_{\text{Pl}}^2}{\mu^2} (\text{Im } \tau)^2 \left| \frac{E_6}{E_4} \right|^2, \\ N_* &= \frac{\Lambda^2}{\sqrt{3} M_{\text{Pl}}} \int dt |j|. \end{aligned} \quad (26)$$

The slow-roll dynamics takes for  $j$ -inflation the form

$$\dot{\phi}^I = \frac{2\pi i^I M_{\text{Pl}}}{\sqrt{3} \mu} \Lambda^2 (\text{Im } \tau)^2 \left( \frac{E_6}{E_4} + (-1)^I \frac{\bar{E}_6}{\bar{E}_4} \right) |j|. \quad (27)$$

The energy scale  $\Lambda$  does not enter  $n_{\mathcal{R}\mathcal{R}}$  or  $r$ , but it does appear in the differential equation, hence the number of  $e$ -folds associated to inflaton trajectories. It can be expressed in terms of  $\mu$  and the amplitude of the primordial CMB amplitude  $A_{\mathcal{R}\mathcal{R}}$  as

$$\Lambda = M_{\text{Pl}} \left( 192\pi^4 \frac{M_{\text{Pl}}^2}{\mu^2} A_{\mathcal{R}\mathcal{R}} (\text{Im } \tau)^2 \left| \frac{E_6}{E_4} \right|^2 \frac{1}{|j|^2} \right)^{1/4}. \quad (28)$$

This leaves the parameter  $\mu$ , and hence the curvature scalar, to be constrained by the cosmological observables. The phenomenological analysis now aims to investigate the target space of  $j$ -inflation.

A more detailed foundational formulation of modular inflation at level one can be found in [7,9], and the generalization from the full modular group  $\text{SL}(2, \mathbb{Z}) = \Gamma_0(1)$  to Hecke congruence subgroups  $\Gamma_0(N)$  at higher level  $N$  has been introduced in Ref. [11].

#### IV. GLOBAL STRUCTURE OF THE POTENTIAL SURFACE OF $j$ -INFLATION

The aim of the preliminary phenomenological analysis of  $j$ -inflation presented in Ref. [9] was to establish the existence of inflaton trajectories that are compatible with the known constraints for the spectral index of the scalar power spectrum, the bound on the tensor power spectrum via the tensor ratio, and the number of  $e$ -folds. Since the bound on the tensor ratio  $r$  established by the CMB satellite probes is small, it is clear from the  $j$ -inflation expression for  $r$  given in Eq. (26) that viable values for  $\phi_*^I$  can be found in the neighborhoods  $U(\tau_s)$  of the zeros of the modular form  $E_6$ . One such zero is at  $\tau_s = i$ . A close-up view of the neighborhood  $U(\tau_s)$  for  $\tau_s = i$ , together with the shape of a typical trajectory, is shown in Fig. 4 of Ref. [9]. The scale of the saddle point at  $\tau_s = i$  is given by the curvature matrix, which for the  $j$ -inflation potential is given by

$$V_{,IJ}(i) = \frac{3 \cdot 432^2 \Gamma(\frac{1}{4})^8 \Lambda^4}{\pi^4 \mu^2} \begin{pmatrix} -1 & 0 \\ 0 & 1 \end{pmatrix}. \quad (29)$$

This curvature matrix immediately gives the mass matrix of the inflaton perturbations at the critical point. Away from the saddle point, the mass matrix receives contributions from terms that depend on the slow-roll parameters. A recent discussion that aims at a characterization of critical points in terms of discrete symmetries in a general context that includes inflationary models can be found in [59].

Attempts have been made to classify single field inflation models by the curvature  $V''$  of the potential [60–64]. A natural way to generalize these early discussions would be by keeping track of the eigenvalue structure of the flat

curvature matrix  $V_{,IJ}$  of the potential or its covariant form  $V_{;IJ}$ . A simpler structure could alternatively be obtained by considering the determinant  $J(V) = \det(V_{,IJ})$  or its covariant form  $J_{\text{cov}}(V)$ . A more phenomenological, but somewhat less structural, characterization however might proceed by the generalization of the single field slow-roll parameter  $M_{\text{Pl}}^2 V''/V$ . In multifield inflation, the analog of this parameter is  $\eta_{IJ} \epsilon^I \epsilon^J / (G^{KL} \epsilon_K \epsilon_L)$ , which is not just a rescaled curvature matrix.

In the present paper, the phenomenological considerations aim at a more global view of the slow-roll phase space, and the structure of the potential surface away from the saddle point  $\tau_s = i$  becomes of interest. One of the main motivations for  $j$ -inflation is the fact that the shift symmetry, often introduced as an *ad hoc* approximate invariance, is now part of a bona fide symmetry of the theory. Modular inflation at level one is invariant under the full modular group  $\text{SL}(2, \mathbb{Z})$  of integral  $2 \times 2$  matrices of determinant one. This infinite group can be generated by just two elements, given by

$$S = \begin{pmatrix} 0 & 1 \\ -1 & 0 \end{pmatrix}, \quad T = \begin{pmatrix} 1 & 1 \\ 0 & 1 \end{pmatrix}. \quad (30)$$

The generator  $T$  shifts the inflaton multiplet, leading to a repetitive pattern of the inflaton field space of the upper half plane  $\tau \in \mathcal{H}$  as  $T$  shifts by one unit  $\tau \rightarrow \tau + 1$ . The investigation of the behavior of modular inflation models can therefore be restricted without loss of generality to bands of width one. In this paper, the focus is on the vertical band bounded by  $-1/2 \leq \tau^1 < 1/2$ .

The structure of the potential surface is simple for larger  $\tau^2$  but becomes more complicated as one approaches the region where  $\tau^2 \rightarrow 0$ . Figure 1 illustrates this with a view that shows a partial region of the embedded surface. This graph indicates a canyonlike structure that emerges as one approaches the boundary of the field space given by the horizontal axis for  $(\text{Im } \tau) = 0$ , with saddle points visible at  $\tau_s = i$  and  $\tau_s = (1 + i)/2$ . Further saddle points exist closer to the boundary but are obscured in this 3D picture. These become transparent in the contour graphs discussed further below. In coordinate space, the slopes steepen as  $\text{Im } \tau \rightarrow 0$ , but the hyperbolic metric stretches the physical distances in field space, thereby flattening the potential surface. This becomes important below in the analysis of the behavior of the trajectories in  $j$ -inflation.

The minimum of the potential is at  $\tau_{\text{min}} = e^{2\pi i/6}$ , which is determined by the zero of the Eisenstein series  $E_4$  in the numerator of the inflaton potential, combined with the fact that at the point  $\tau_{\text{min}}$  the Ramanujan modular form  $\Delta(\tau)$  that appears in the denominator of  $V$  does not vanish. As the component  $\phi^2$  of the inflaton doublet increases beyond the saddle point at  $\tau_s = i$ , the  $j$ -inflation potential forms a wall and diverges. This can be seen explicitly from the definition of the Eisenstein series given in Eq. (15).

As  $\text{Im } \tau \rightarrow \infty$ , the variable  $q = e^{2\pi i \tau}$  vanishes, and the Eisenstein series approach unity in the normalization adopted here. Since the Ramanujan form approaches  $q$  in this limit, the  $j$  function diverges.

The trajectories of the inflaton evolution considered in [9] all originated in the neighborhood  $U(\tau_s)$  of the saddle point at  $\tau_s = i$ . The evolution of those orbits was such that it lasts long enough to produce sufficient inflation and is furthermore compatible with the observational results of the CMB probes. Figure 1 shows that there are other saddle point regions and that the potential surface of  $j$ -inflation has an intricate structure that the large scale three-dimensional representation of the surface does not display in full detail. Better insight into the potential surface can be obtained by representing the 3D potential shown in Fig. 1 in a contour plot, as in Fig. 2. This graph not only shows the saddle point region considered in [9], as well as the structures in Fig. 1, but also shows a number of further saddle points on both sides of the ridge of the saddle point  $\tau_s = i$ . A zoom of the above contour plot in the lower panel of Fig. 2 shows that the potential becomes more complicated as one approaches the horizontal axis, i.e., the boundary of the target space. This structure is reminiscent of a fractal pattern, but the picture suggested by this graph has to be complemented by the behavior of the hyperbolic metric, which diverges as the saddles approach the real axis.

The precise degree of detail obtained in the plots of the  $j$ -inflation potential depends on the resolution and also on the accuracy with which the potential is computed. This is relevant because the modular forms involved in the definitions of the  $j$  function are infinite series which have to be truncated. An increase of the number of terms increases the amount of detail that can be seen; thus, the order to which the

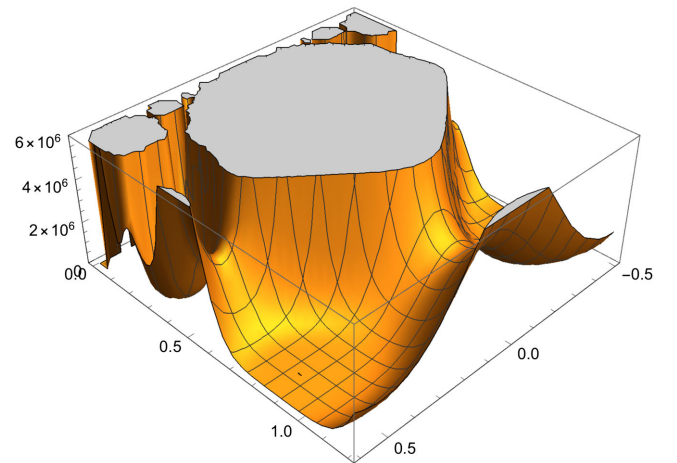


FIG. 1. A large scale view of the  $j$ -function surface  $|j|^2$  (the energy scale parameter  $\Lambda$  is determined by the CMB amplitude  $A_{\mathcal{R}\mathcal{R}}$ ). The plot shows two of the saddle point regions, one of which has a mirror on the far side of the graph. The minimum of the potential is located at  $\tau_{\text{min}} = e^{2\pi i/6}$ .

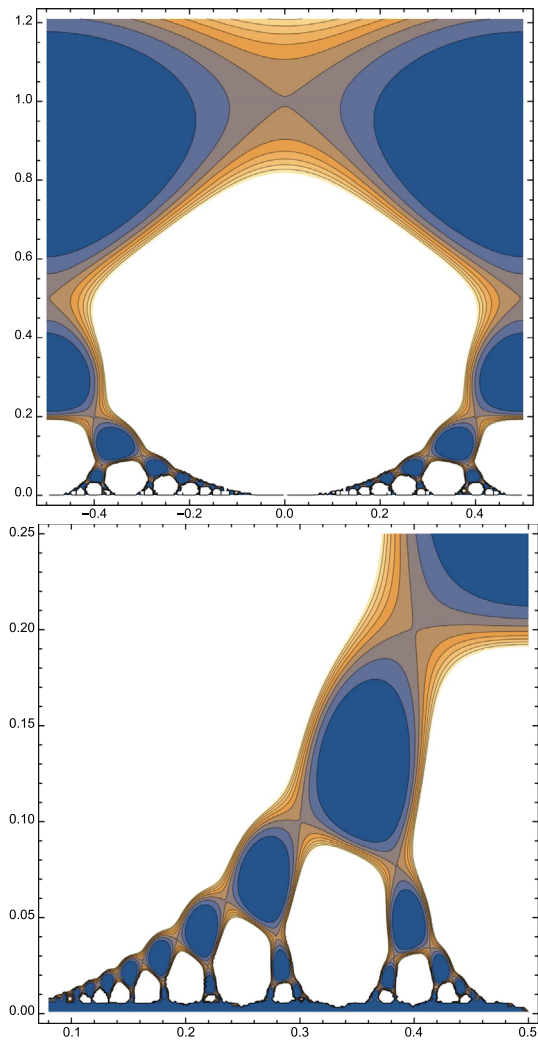


FIG. 2. Contour lines of the potential surface modulo the energy scale. Deep blue indicates the low regions of the potential in this 2D contour projection, while the lighter colors indicate higher elevations of the potential. The white regions represent horizontal cuts beyond which no new saddle points appear, and the structure of the potential is irrelevant for the present discussion. This graph shows that there are further saddle point regions when  $\tau^2 = \text{Im } \tau$  approaches the boundary of the target space, determined by  $\tau^2 = 0$ . The ridge toward the top of the upper panel shows the region around the saddle point  $\tau_s = i$  which was the main focus of Ref. [9].

Eisenstein series are computed needs to be adjusted depending on how close to the real axis the computation should proceed. An increase of the accuracy of course means longer CPU times.

## V. LARGE AND SMALL FIELD INFLATION IN HYPERBOLIC $\sigma$ MODELS

One of the longstanding issues in inflation is the dichotomy between large field and small field inflation, emphasized, for example, by Lyth in the context of single

field inflation [65]. These discussions revolve around the relation between the distance covered by the inflaton in field space and the tensor ratio, mediated by the number of  $e$ -folds during inflation. In multifield inflation, this relation is less direct because the distance in field space involves not only changes of the fields  $\Delta\phi^I$  but also depends on the metric  $G_{IJ}$  of the target space. It is therefore useful to separate issues pertaining to the field values from those that depend on the distance in field space, hence, in general, involve the metric.

Part of the current discussion that informs the planning and construction of the next generation experiments aiming to discover the contribution of inflationary tensor modes to the CMB is the formulation of significant targets for the tensor ratio  $r$ , which is discussed in detail in Sec. X. Tensor mode targets that have been identified in recent years have been motivated by distinguishing between models with inflaton values that are either super- or sub-Planckian. This distinction has, in particular, led to the formulation of classes of single field inflation models along these lines in the hope that this leads to the identification of more generic characteristics of inflationary models that might be testable with CMB data (early work in this direction can be found in Refs. [60–64]). The demarcation line between these two classes is not precise, but this lack of precision is not important for the following. What is of interest is the common association in the literature of large field inflation with large  $r$  and small field inflation with smaller  $r$ . These discussions raise the question whether a similar behavior can be identified in multifield inflation, in general.

In  $j$ -inflation, there are two aspects that arise in this context. The first of relevance, in principle, for any multifield framework, is that the different components of the inflaton multiplet can have rather different scales, making the distinction of sub-Planckian vs. super-Planckian field values less a feature of the field itself, even though it still retains its importance for at least some components. This is the case in  $j$ -inflation in neighborhoods  $U(\tau_s)$  of the saddle point  $\tau_s = i$ . For initial values  $\tau_*$  in  $U(i)$ , at least one of the field values is super-Planckian for  $\mu > M_{\text{Pl}}$ . Hence, the vertical component is large  $\phi_*^2 \cong \mu$ , while the horizontal component  $\phi_*^1$  can be much smaller, depending on how close to the saddle point  $\phi_s$  the initial value  $\phi_*$  is. In this case, the general philosophy can be applied by a slight change of formulation.

A second feature, specific to the modular inflation framework, is that modular transformations connect an infinite number of different regions of the target space. This also applies more generally to automorphic inflation. The contour plots in Fig. 2 show sequences of critical points of the  $j$ -inflation potential that form arcs oriented toward the origin of the  $\tau$  plane. These saddle point regions can be mapped with elements of the modular group  $\text{SL}(2, \mathbb{Z})$ , which is generated by the elements  $S$  and  $T$  in Eq. (30). The top arcs in the upper panel of Fig. 2 can be reached, for

example, from the saddle point at  $\tau_s = i$  with the sequences of group elements,

$$(TST)^{\pm n}(i) = \pm \frac{n}{n^2 + 1} + \frac{i}{n^2 + 1}. \quad (31)$$

These representations of the primary arcs are not unique because  $Si = i$ ; hence, these primary sequences can be obtained with a number of different group elements.

The next sequences of saddle points, both illustrated in the upper panel, but more clearly visible in the zoom in the lower panel, can be obtained via

$$\begin{aligned} (TST)^n T(i) &= \frac{2n+1}{2n^2+2n+1} + \frac{i}{2n^2+2n+1}, \\ ST^n(TST)(i) &= -\frac{2n+1}{2n^2+2n+1} + \frac{i}{2n^2+2n+1}. \end{aligned} \quad (32)$$

The general picture illustrated by these maps is that modular invariance of the  $j$  potential leads to saddle points  $\tau_n$  obtained by maps  $\gamma_n$  obtained from elements in the modular group.

The main feature of these maps  $\gamma_n$  is that they approach the origin  $\tau = 0$  ever closer as  $n$  increases, which is apparent for the images of the  $\tau_s$  in (31) and (32). For more general  $\tau$ , this can be illustrated with the sequences  $\gamma_n$  obtained, for example, by the iteration of a generating element  $\gamma$  as  $\gamma_n = \gamma^n$  for the group element  $\gamma = TST$ . These maps  $\gamma_n$  send arbitrary points  $\tau$  to images of the form

$$\gamma_n(\tau) = \frac{\tau^1 + n|\tau|^2 + i\tau^2}{1 + 2n\tau^1 + n^2|\tau|^2}, \quad (33)$$

generalizing the sequence (31) of the saddle point  $\tau_s = i$ . For an initial value  $\tau_*$  in a neighborhood of  $\tau_s = i$ , this sequence converges to the origin of the  $(\tau^1, \tau^2)$  plane, and in the process, sends both components  $\tau_*^l$  to ever smaller field values. The existence of such sequences that approach the origin of the field space shows that it is possible to have viable  $j$ -inflation trajectories that start with sub-Planckian field values.

The implication of these sequences of maps  $\gamma_n$  is that large field initial values  $\tau_*$  in a neighborhood of the large field saddle point  $\tau_s = i$  with larger tensor ratios  $r(\tau_*) \geq 0.01$  (which satisfies the PLANCK bound) are mapped into small field initial values  $\gamma_n(\tau_*)$  with the same tensor ratio,

$$r(\gamma_n(\tau_*)) = r(\tau_*). \quad (34)$$

In Sec. X, it is shown that, depending on the parameters of the model,  $j$ -inflation can lead to tensor ratios that reach the current bound reported by the PLANCK Collaboration but can also reach down to the target range of upcoming experiments, such as the Simons Observatory and the CMB-S4

experiment. Combined with the discussion above, this shows that in  $j$ -inflation, and *eo ipso* in multifield inflation, small field inflation can lead to large tensor ratios, and large field inflation can lead to small tensor ratios.

## VI. $j$ -INFLATION TRAJECTORIES AND HYPERBOLIC GEODESICS

The analysis discussed in the next section shows that sufficient inflation takes place in a large volume of the field space of  $j$ -inflation. It is in this context of interest to investigate in more detail the behavior of the inflaton trajectories in different regions of the target space. The geometry and the physics of the orbits depends of course on the potential surface above the target space. In particular the structure of the regions with sufficient inflation, or the existence of attractors, is dependent on the form of the potential, hence necessitates the consideration of inflaton trajectories on the potential surface. The inflaton behavior can also be considered in the field space itself by projecting the inflaton paths down to the target space, where they can be compared with the geodesics defined by the target space metric, in the present case the hyperbolic metric of the upper half plane. The latter comes in two types, straight vertical lines and semicircles, and the natural question is how the inflaton trajectories compare to the geodesic paths. Naively, one might expect the geodesic motion in the field space to be irrelevant in slow-roll inflation because it is the gradient structure of the potential that is important, and the dynamics of the inflaton itself even along approximately geodesic paths will depend on the potential. However, it becomes clear below that sufficient inflation can be achieved with a family of inflaton orbits that interpolate between the two types of hyperbolic geodesics.

### A. Hyperbolic geodesics and the effect of modular dynamics

A natural question in the case of curved target spaces is how the physical geometry of the field space differs from the purely geometric dynamics, i.e., in what way the inflaton potentials affect the trajectories projected down to the target space as compared to the geodesics. This is also of interest in the context of how the swampland conjectures might relate to the observational bounds on  $r$  because the former are concerned in part with geodesic distances while the latter impact the distances along inflaton trajectories. The geodesic equations for the upper half plane  $\mathcal{H}$  lead to the coupled system given by

$$\begin{aligned} \tau^{1''} - \frac{2}{\tau^2} \tau^1 \tau^{2'} &= 0, \\ \tau^{2''} + \frac{1}{\tau^2} (\tau^1)^2 - (\tau^{2'})^2 &= 0, \end{aligned} \quad (35)$$

where the dimensionless variables  $\tau^l$  are used, and the

primes denote the derivative relative to the dimensionless time. These equations can be solved in terms of straight vertical lines  $\tau^1 = \text{const}$  as well as by semicircles that intersect the  $\tau^2 = 0$  axis vertically, i.e., with centers along the real axis. Parametric forms of these geodesics can be obtained in two different ways, using either a group theoretic parametrization or a formulation in terms of hyperbolic functions. More precisely, the geodesic solutions can be given as a combination of a pair of maps of the point  $\tau = i$  defined by elements  $\beta_t, g$  in the Möbius group as

$$\tau_g(t) = g \circ \beta_t(i), \quad (36)$$

where

$$\beta_t := \begin{pmatrix} e^{t/2} & 0 \\ 0 & e^{-t/2} \end{pmatrix}, \quad g = \begin{pmatrix} a & b \\ c & d \end{pmatrix} \in \text{SL}(2, \mathbb{R}), \quad (37)$$

and the action is given as usual by the fractional transformation. The identity  $g = \text{id}$  leads to vertical geodesics on the imaginary axis  $\tau = e^t i$ , and the shift matrices generate other vertical lines. This shows that the upper half plane  $\mathcal{H}$  is a geodesically complete manifold. The group theoretic geodesics (37) can be mapped into the hyperbolic function parametrization that provides an alternative parametrization of the semicircle geodesics.

In Figs. 3 and 4 inflaton trajectories are shown for initial values both in the neighborhood of the critical point  $\tau_s = i$  and in a more global region. Figure 4, which will also be relevant for the attractor discussion of the next subsection, shows a collection of trajectories in the fundamental strip. It establishes that for a wide range of initial values the potential of  $j$ -inflation, and hence modular inflation, in general, has an important effect on the specifics of the dynamical solutions. Even with the constraint imposed on the number of  $e$ -folds, the  $j$ -inflation trajectories form a continuous family that turns from the vertical line type of geodesics into the semicircle type of geodesics. For initial values with large  $\text{Im}\tau$  and  $\text{Re}\tau$  closer to the boundary of the central vertical band, the trajectories approximate the vertical geodesics, while for initial values closer to the saddle point  $\tau_s = i$ , they eventually approximate the semicircle geodesics. In the process of this interpolation, the family of trajectories inevitably contains paths that are far from being of geodesic type.

If one imposes further phenomenological constraints such as the spectral index and the tensor ratio, the  $j$ -inflation initial values are forced to start closer to the saddle points, as illustrated by a selection of different trajectories in Fig. 3. These paths show that during the early phases of  $j$ -inflation even those trajectories that are compatible with the PLANCK constraints for the spectral index and the tensor ratio can have interesting dynamical behavior that deviates from the geodesic. On the other hand, there do exist trajectories in  $j$ -inflation that approach the geodesic very quickly. This

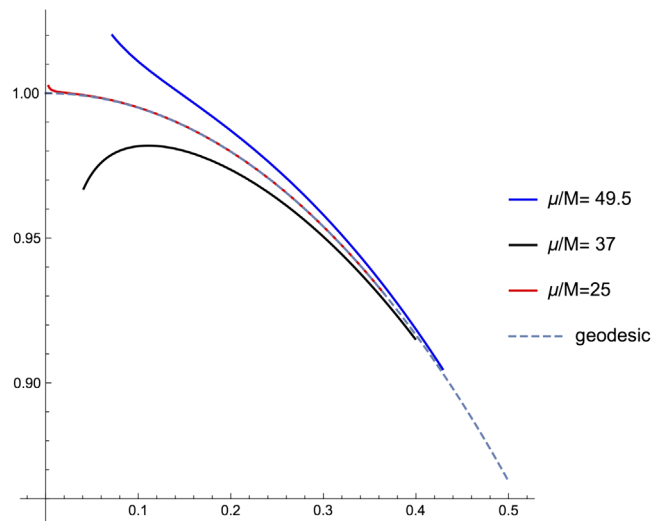


FIG. 3. An illustration of  $j$ -inflation trajectories in the  $(\tau^1, \tau^2)$  target space for different energy scales  $\mu$ . The dashed curve shows the geodesic that connects the saddle point  $\tau_s$  with the minimum of the  $j$ -inflation potential. As before, these  $j$ -inflation trajectories are truncated at the end of inflation, but the geodesic is tracked to the minimum of the potential.

comparison of course only concerns the geometric form of the paths involved. Physically, the potential surface is still important even for trajectories that are close to being geodesic because it is the potential that determines the timescales of the inflaton dynamics.

Figure 3 also provides another illustration of the attractor nature of the inflationary trajectories on a more local scale. If one continues to follow the dynamics along these orbits, they all converge onto the geodesic path that connects the saddle point  $\tau_s = i$  with the minimum of the  $j$ -inflation potential. This feature is enhanced for trajectories that originate close to the saddle point.

## B. Attractorlike behavior

In the context of the issue of fine-tuning of initial conditions, it is natural to ask whether inflationary models show features that are reminiscent of attractor behavior for inflaton trajectories. The mathematical concept of an attractor involves large time behavior [66]; hence, strictly speaking, it is not applicable in models in which inflation ends after a finite time, whatever the mechanism. It is nevertheless of interest to ask whether an inflationary potential has basins into which inflaton trajectories with quite different initial conditions tend to converge and whether the trajectories that converge to these basins have similar physical parameters. For single field inflation, there is a large amount of literature on this topic, and for a special class of models, this is discussed briefly in the recent reviews [67,68] and references therein. In the framework of multifield inflation, attractors have received less attention, but a recent analysis can be found in [69].

In light of these discussions, it is of interest to consider trajectories in  $j$ -inflation.

The illustration of the potential in Fig. 1 shows that it increases and forms a wall for large imaginary components of the inflaton doublet. One can ask what the trajectories are that these initial conditions with sufficient inflation lead to, and Fig. 4 shows a selection of  $j$ -inflation initial values and their associated trajectories. The paths in this graph all lead to inflation within the canonical range for the number of  $e$ -folds  $N_* \in [50, 70]$  adopted in the present paper, and they are tracked to the end of inflation.

Included in Fig. 4 are also trajectories that start in the neighborhood of saddle points of the potential that are closer to the real axis. These trajectories appear to be much shorter in the coordinate space variables of this graph, but because of the nontrivial hyperbolic metric of the field space, the physical lengths of these paths are larger since they are closer to the horizontal axis. The factor  $(1/\text{Im}\tau)$  in the length  $ds$  leads to an ever stronger stretching as  $\text{Im}\tau$  approaches zero.

The trajectories in Fig. 4 show that sufficient inflation can be obtained in  $j$ -inflation for a wide variety of different types of trajectories. Along some of these orbits, either of the two components  $\tau^I$  of the inflaton can be approximately constant, which is an assumption that is sometimes made in the two field inflation literature. There are however also trajectories for which both of the components vary considerably; hence, in  $j$ -inflation, sufficient inflation can be

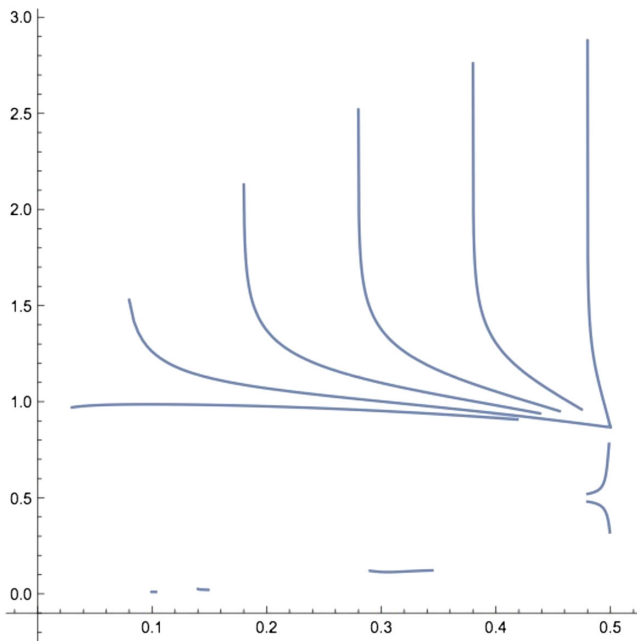


FIG. 4.  $j$  Inflaton trajectories in the  $(\tau^1, \tau^2)$  target space plane for  $\tau^1 \in [0, 1/2]$ . The  $e$ -folds for these trajectories in field space are all in the standard range  $N_* \in [50, 70]$ . The hyperbolic metric rescales the physical length of these paths drawn in the diagram.

obtained along trajectories that represent true two field inflation.

The paths shown in Fig. 4 also illustrate how the trajectories that originate close to the saddle point  $\tau_s = i$  serve as attractor basins into which a continuum of trajectories merge that start away from the saddle point. This behavior extends even to trajectories that start higher up the wall region of the potential. Only orbits that approach the linear type geodesics when projected down onto the field space approach the minimum in a more direct way. Their structure approximates vertical geodesics, which are briefly described above.

## VII. SUFFICIENT INFLATION

The question whether a given field theoretic model might be useful in an inflationary context is usually posed in a first iteration as a constraint on the lower bound on the number of  $e$ -folds  $N_*$ . The original motivation for inflation leads to a rough estimate for  $N_*$ , and a number of investigations of different models involving an inflaton doublet have focused on an analysis of the phase space that leads to sufficient inflation in this sense. A model that has received particular attention over the years is hybrid inflation [36], and papers that report results of such scans include [37–43]. Inflation must end eventually, and in principle, such scans of the phase space should impose also an upper bound for  $N_*$ .

The duration of inflation has received much attention in the literature, not only because it is the parameter that is most immediately relevant for the puzzles that initially played an important role in the introduction of the inflationary framework, but because it has also served as a focal point to provide more precision to the question of how probable inflation is, for example, in the formulation of Gibbons and Turok [49]. It has turned out to be difficult to constrain the number of  $e$ -folds precisely, in part because it depends on the choices that have to be made to account for the postinflationary evolution. The main uncertainty in determining a definite range is the reheating stage, which is poorly constrained observationally and which is complicated because of its preheating phase during the early stages of this process. Despite much work on issues related to preheating, no clear estimates for the number of  $e$ -folds and the reheat temperature have emerged. Consequently, the range of  $e$ -folds that has been considered in the literature covers a wide range, reflecting the lack of constraints on the energy scales that are allowed in this context, reaching from a lower bound given by the nucleosynthesis scale of some (1–10) MeV, to the GUT scale of  $10^{16}$  GeV. Given a choice for the accepted range of the number of  $e$ -folds, i.e., a choice of the evolutionary scenario, a key issue to address is whether the given model under discussion provides enough inflation in the adopted framework. In the absence of better constraints on the postinflationary stages, a canonical range for the number of  $e$ -folds  $N_*$  between horizon crossing and the end of inflation has emerged that posits that from 50 to 60 is

a reasonable minimal value for  $N_*$ . Such values were, for example, imposed as a lower bound in the work on hybrid inflation. In the present analysis of  $j$ -inflation, more specific bounds for the number of  $e$ -folds are implemented.

### A. Initial conditions in $j$ -inflation for sufficient inflation

In the present paper, a conservative range for the number of  $e$ -folds is chosen as  $N_* \in [50, 70]$  to define viable realizations. Using this as a constraint on  $N_*$ , the existence of trajectories in  $j$ -inflation with enough inflation was established in [7,9]. (The generalization to higher level models was considered in [11].) A systematic scan of the slow-roll phase space is computationally expensive at high resolutions of the field space, with most of the time spent on the computation of the number of  $e$ -folds  $N_*$ . A balance thus has to be found between the resolution of the lattice in inflaton space as well as the time resolution used in the determination of the end of inflation  $t_e$ . By choosing the inflaton resolution  $\delta\tau^l = \delta\phi^l/\mu$  low enough, it is possible to scan the central vertical band out to a range of  $\text{Im}\tau$  where the  $e$ -folds fall outside of the adopted range. A typical scan of the initial values leads to a structure that is reminiscent of a butterfly, as shown in Fig. 5.

The feelers of the butterfly distribution reflect the intricate structure of the potential surface as one approaches the horizontal axis  $\phi^2 = 0$  that defines the boundary of the modular inflation field space. This structure is indicated in the 3D plot of Fig. 1 and can be seen more clearly in the global contour plot of Fig. 2. A discussion of the behavior of the inflaton trajectories corresponding to these initial values has been given in the previous section. The structure of the 2D butterfly can be explained by resolving the graph by adding the number of  $e$ -folds  $N_*$  as a third dimension. Figure 6 shows that the upper and lower boundaries of the butterfly structure are determined by the bounds on the number of  $e$ -folds. They are obtained because, when moving

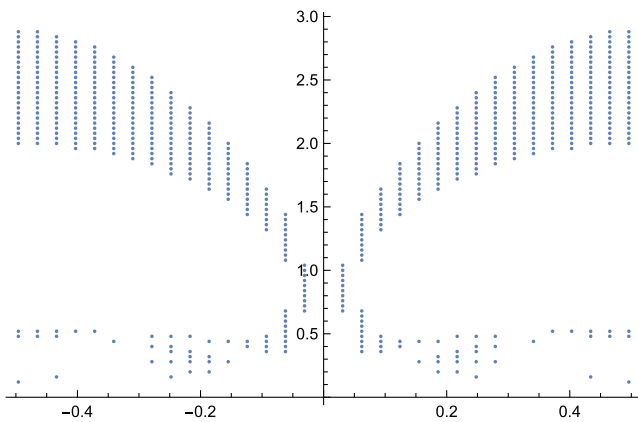


FIG. 5. The butterfly graph in the  $(\tau^1, \tau^2)$  target space in the fundamental band  $\tau^1 \in [-1/2, 1/2]$ . The butterfly boundaries are determined by the constraints on the number of  $e$ -folds  $N_* \in [50, 70]$ . See also Fig. 6 for more detail.

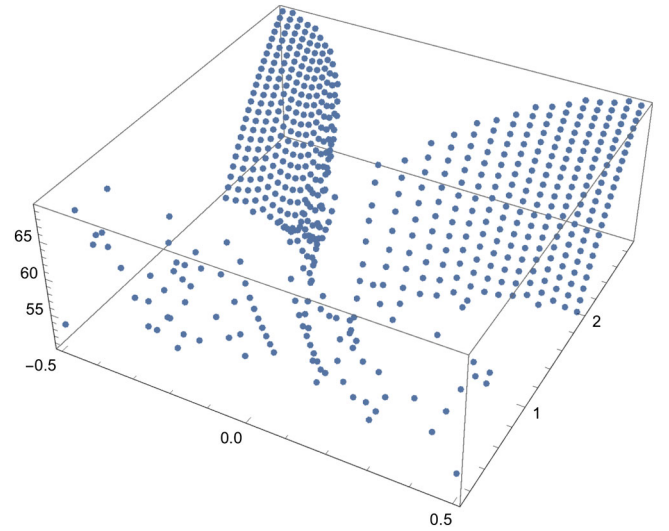


FIG. 6. The 3D function of the  $e$ -fold number  $N_*$  along the vertical axis on the dimensionless target space  $(\tau^1, \tau^2)$  for  $e$ -folds in the range  $[50, 70]$ . This graph shows that the upper and lower boundaries of the butterfly wings are determined by the upper and lower limits adopted for the number of  $e$ -folds. Varying these limits will vary the boundaries of the butterfly.

away from of the thoraxlike structure that appears close to the ridge of the potential along the imaginary axis, the  $e$ -folds produced by the potential are below the lower bound of the interval  $N_* \in [50, 70]$  in the lower region of the target space and above the upper bound in the upper region of the butterfly wings. Varying the bounds for the  $e$ -folds therefore varies the wing boundaries accordingly.

### B. A natural measure on the space of initial conditions

A question often raised in the context of inflation is how much of the space of initial conditions actually leads to inflation. The answer to this question involves some kind of measure that needs to be chosen. For general multifield inflation with a curved field space, the target space comes equipped with a natural measure given by the volume measure  $\omega = \sqrt{\det G_{IJ}} \prod_K d\phi^K$ . Even though, in general, the volume of a noncompact space will diverge in this measure, the situation is different in modular inflation, where the metric measure provides a finite volume for the fundamental domain of the target space. There are two features of modular inflation that combine to allow the computation of a finite fraction of the initial conditions that lead to sufficient inflation. The first is that the modular symmetry constructs the full target space as an infinite number of copies of the irreducible fundamental domain  $\mathcal{F}$  of the upper half plane  $\mathcal{H} \subset \mathcal{H}$ , given by

$$\mathcal{F} = \mathcal{H}/\text{SL}(2, \mathbb{Z}), \quad (38)$$

which extends infinitely high along the imaginary axis in the interval  $[-1/2, 1/2]$ . The second feature is that the

metric is given by (11), and while the euclidean area of  $\mathcal{F}$  is infinite, the hyperbolic metric provides a finite area for the fundamental domain, given by

$$\text{vol}(\mathcal{F}) = \int_{\mathcal{F}} \sqrt{\det G} d\phi^1 d\phi^2 = \frac{\pi}{3} \mu^2 = -\frac{2\pi}{3} \frac{1}{R_{\text{fs}}}. \quad (39)$$

It becomes clear in the later sections that the CMB data constrains  $\mu$  and hence the physical area of the fundamental domain.

Given that the volume of the fundamental domain  $\mathcal{F}$  is finite, it is natural to consider the quotient of the butterfly volume and the total volume as a measure of the likelihood of  $j$ -inflation with a number of  $e$ -folds in the canonical interval. This quotient can be interpreted as the probability for  $j$ -inflation to produce  $N_* \in [50, 70]$   $e$ -folds. It can also be interpreted as the posterior probability by assuming that the prior probability distribution is constant, which allows one to cancel it in Bayes' theorem. As a result, modular inflation leads to the probability

$$P(N_* \in \mathcal{I}) = \frac{\text{vol}(B_{\mathcal{F}})}{\text{vol}(\mathcal{F})}. \quad (40)$$

A rough estimate of the volume of  $B_{\mathcal{F}}$  shows that a large fraction of the total field space leads to inflation in the range considered here. In the literature, the probability of inflation is often discussed by setting a lower cutoff for  $N_*$ ; for example,  $N_* \geq 60$ , see, e.g., papers [37,38,40–42,44], where the space of initial conditions with  $N_* \geq 60$  is analyzed for hybrid inflation. The structure of  $j$ -inflation is such that if one lets  $N_*$  grow unbounded then the probability approaches one.

### C. Finite measures of modular inflation and the swampland conjectures

In the past, the question of how likely inflation is has often been phrased in terms of measures that are not normalizable, leading to regularization issues [47,48,50,51]. It is worthwhile to note here that the conjectures that have been formulated in the context of the swampland conjectures place modular inflation in a larger framework in which the existence of a geometric measure on the target space is guaranteed by fiat.

The swampland conjectures have been introduced as an attempt to formulate criteria for effective field theories that can be embedded in a theory of quantum gravity. For the most part, it is assumed that this theory is string theory, and much of the work aimed at providing evidence for the conjectures has been done within this framework. A review of recent work can be found in [70], and further work on the impact of these conjectures on inflation includes [71]. However, the formulation of at least some of the criteria considered so far takes place within the effective field theory and does not directly refer to string theoretic features.

Among the earliest constraints imposed were conditions extrapolated by Ooguri and Vafa [72] from the behavior of string theory moduli. These can be rephrased in terms of inflationary scalar fields, independent of any moduli interpretation. The focus of these early considerations was on the topological and geometric structure of target space of the scalar fields, in general, a multicomponent field  $\phi^I, I = 1, \dots, n$ . The topological conjecture states that the target space is noncompact in the sense that there exist trajectories of infinite length. The precise length of these trajectories depends on the form of the distance measure [73], but this does not affect the basic picture of the topological conjecture. Figure 4 illustrates the existence of such paths as one increases the imaginary range of the inflaton doublet indefinitely.

The geometric conjecture posits that despite the non-compactness the target space has finite volume. What is assumed implicitly in such statements is that the focus is on the fundamental domain. In this context,  $j$ -inflation, and more generally modular inflation, are examples of theories that satisfy the finite volume conjecture [74,75], as discussed above.

There are further conjectures that are currently under discussion in the literature. At this time, no consensus has been reached about the significance of these postulates, which eventually may pave the way to reformulations of inflation or alternative models, see, e.g., [76–81].

## VIII. SPECTRAL INDEX FUNCTION $n_{\mathcal{R}\mathcal{R}}$ ON THE FIELD SPACE

One of the fundamental parameters that has been determined with a dramatic increase in precision by the post-COBE satellite experiments is the adiabatic spectral index  $n_{\mathcal{R}\mathcal{R}}$  of the curvature Lukash-Bardeen perturbation  $\mathcal{R}$ . The specific value and uncertainty of the spectral index depends on the details of the fits. For the most part, the fits that have been published by the collaborations are aimed at single field inflation, and the parameter space is correspondingly lower dimensional. Fits that are aimed at two field inflation usually adopt special types of parametrizations for the scalar power spectrum and often make assumptions concerning the correlations between the adiabatic and the isocurvature perturbation. Currently, no multifield specific fit of the final PLANCK data release has been performed, but extended fits beyond the minimal parameter count have been obtained in Ref. [82]. In the present paper, bounds are used that are close to the PLANCK values.

In  $j$ -inflation the spectral index  $n_{\mathcal{R}\mathcal{R}}(\tau^I)$  is given by the fairly complicated function in Eq. (26) in terms of the Eisenstein series. The analytic structure of this function is not immediately transparent, but its geometry can be determined numerically and is shown in Fig. 7. The structure of this surface explains some of the features of the numerical scans for viable initial conditions that satisfy not only the

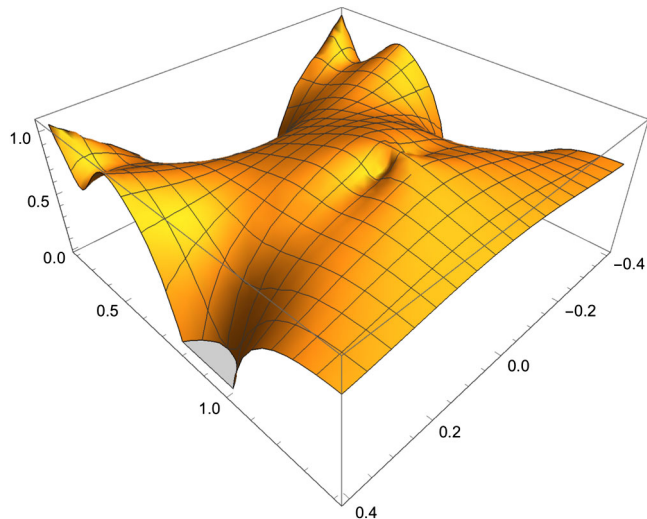


FIG. 7. Large scale view of the spectral surface  $n_{\mathcal{R}\mathcal{R}}(\tau^1)$ .

constraint on the number of  $e$ -folds but are also consistent with the results from the CMB probes.

### A. $n_{\mathcal{R}\mathcal{R}}$ scans of the field space

It follows from the  $j$ -inflation expressions for the spectral index and the tensor ratio in Eq. (26) that the initial values in the neighborhood of the saddle points  $\tau_s$  are good candidates that might lead to viable trajectories. The region around  $\tau_s = i$  was the focus of the phenomenological analysis of  $j$ -inflation of [9], which established the existence of viable trajectories. In the present section, the focus is on the constraints imposed on the target space by the spectral index as the inflaton ranges over this space for a fixed energy scale  $\mu$ . The effect of the variation of  $\mu$  on the spectral index is considered later in this paper. The results of a global scan of the target space is shown in Fig. 8 superimposed on the contour plot of the potential. This illustrates in some detail the canyonlike structure of the field space close to the boundary.

This global map indicates a chainlike iterative structure of saddle points which can be resolved only to a limited degree in the region very close to the real axis. In order to obtain a more detailed view it is useful to construct a zoom for smaller values of the vertical component of the inflaton. In Fig. 9 the focus is on the region to the right of the ridge, for which this higher resolution graph shows a more detailed structure as one approaches the real axis, in particular, a double sequence of arcs made of saddle point regions that range from the right boundary of the central vertical band toward the origin of field space. These regions come in two different orientations, which are roughly diagonal and off diagonal. Three different arcs are clearly visible, and a fourth one is indicated. The amount of detail visible in such runs depends on the size of the lattice used to scan the field space, as well as the accuracy with which the Eisenstein series are computed.

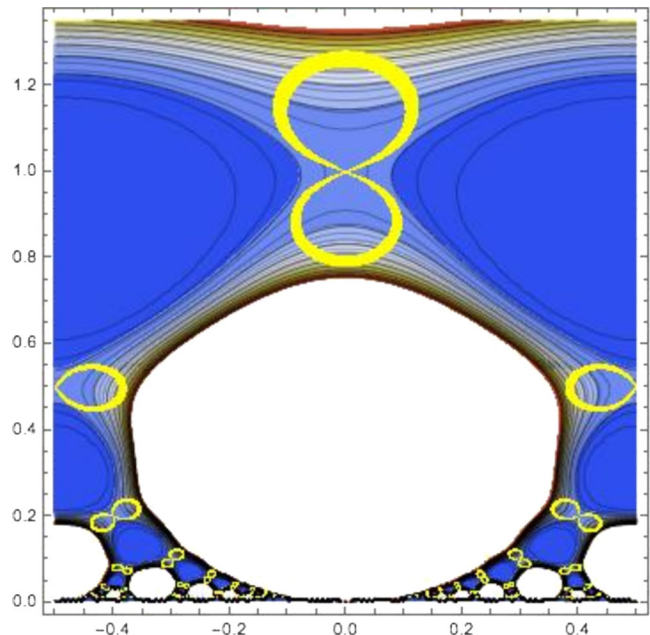


FIG. 8. A scan for viable spectral indices on the field space contour plot of Fig. 2. Here, the target space is again restricted to the fundamental band. The yellow bands illustrate the regions with viable  $n_{\mathcal{R}\mathcal{R}}$  values.

## IX. SCALING BEHAVIOR OF THE SPECTRAL INDEX

A question that has been raised many times in the inflation literature is whether it is possible to derive constraints for the amplitude of the gravitational contribution to the CMB background, given some plausible assumptions. The idea has been to abstract some general behavior from simple models that allows one to deduce, in particular, a lower bound for the tensor-to-scalar ratio  $r$  considered by the CMB collaborations [1–3]. One strategy that has been adopted in single field inflation is to assume some scaling behavior of the equation of state parameter and to consider the implications that result [53]. This

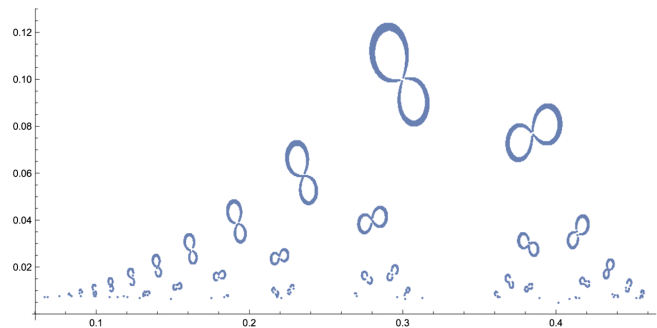


FIG. 9. A zoom of the lower region of the right part of Fig. 8. This shows a highly resolved picture of the Fig. 8 bands that are swept out by the spectral index constraint on the inflaton space  $(\tau^1, \tau^2)$ .

translates immediately into an assumption for the scaling behavior of the slow-roll parameters and hence the spectral index and the tensor ratio. Given the CMB constraints on the spectral index, this translates into estimates for  $r$  [53,55].

In single field inflation, such a scaling behavior is immediate in some simple models. In the class of monomial inflation models [83], the spectral index,

$$n_{\mathcal{R}\mathcal{R}} = 1 - 6\epsilon_V + 2\eta_V, \quad (41)$$

simplifies because of the relation  $\epsilon_V = 2(p-1)\eta_V/p$ , with  $p$  the monomial exponent, as well as the fact that the slow-roll parameter  $\epsilon_V$  can be written in terms of the number of  $e$ -folds as  $\epsilon_V \cong 1/N$ . This leads to the scaling relation,

$$n_{\mathcal{R}\mathcal{R}} \cong 1 - \frac{\alpha_p}{N}, \quad (42)$$

where  $\alpha_p = (p+2)/p$ . This type of relation also holds approximately for different classes of models, for example, the Starobinsky model [84]. For about  $N = 60$   $e$ -folds, the resulting spectral index is consistent with the CMB constraints that have been determined in recent years by the WMAP and PLANCK satellites. The question can be raised whether this scaling holds for some range of  $N$  away from the specific value  $N = 60$ , often adopted as the canonical value.

As noted above, such scaling relations were assumed to hold in attempts to put constraints on the undetermined, but bounded, tensor-to-scalar ratio  $r$ . It was, in particular, observed by Mukhanov [53] that the observational bounds obtained by the WMAP satellite for the spectral index [85], in combination with a relation like (42), allow one to determine lower bounds on the tensor-to-scalar ratio  $r$  (see also the papers [54,55]). This raises the question whether such a relation might be valid more generally in the framework of multifield inflation. In this case, there are, in general, no analytical formulas for  $N$ , and hence, there is no easy access to analytical scaling relations. However, the analysis presented above of the behavior of  $j$ -inflation allows one to address this issue.

In order to test whether the above scaling relation for  $n_{\mathcal{R}\mathcal{R}}$  holds more generally in multifield inflation, it is useful to define the function

$$f_\alpha(n_{\mathcal{R}\mathcal{R}}, N) = n_{\mathcal{R}\mathcal{R}} - \left(1 - \frac{\alpha}{N}\right) \quad (43)$$

for some constant  $\alpha$  and consider the correlation of this functions with the spectral index. If the scaling relation above holds, the function  $f_\alpha$  vanishes. The analysis of the scaling relation in  $j$ -inflation shows that the values of the function  $f_\alpha$  for  $\alpha$  of order one are small, of the order of a few percent. This is illustrated by the graph in Fig. 10. While the function  $f_\alpha$  is small, the behavior of the tensor ratio  $r$  further

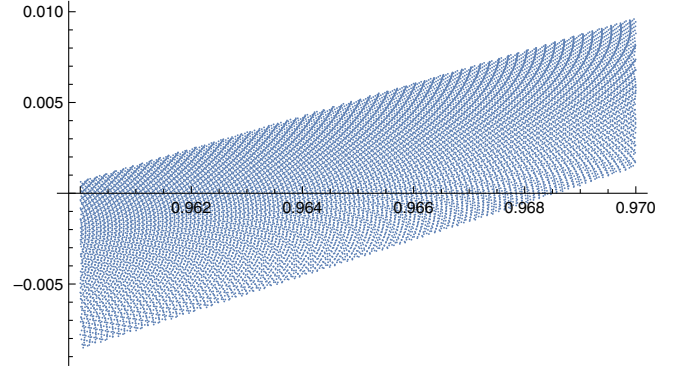


FIG. 10. Typical graph for the function  $f_\alpha$ , plotted along the vertical axis, in dependence of the spectral index  $n_{\mathcal{R}\mathcal{R}}$ , plotted along the horizontal axis. This graph is obtained from the initial values that are consistent with the tensor ratio bound and the canonical range for the  $e$ -folds. The narrowness of this band establishes that the spectral index does follow quite closely the scaling behavior of single field monomial inflation.

above shows that the bounds on  $r$  obtained in the framework of single field inflation are not valid in multifield inflation.

## X. THE TENSOR-TO-SCALAR RATIO FUNCTION $r$ ON THE FIELD SPACE

One of the fundamental phenomenological parameters that constrain inflation is the power amplitude of primordial gravitational waves. This is conventionally quantified by the CMB collaborations in terms of the tensor-to-scalar ratio  $r$  defined in Eq. (6). For  $j$ -inflation, this parameter becomes a function of the energy scale  $\mu$  that determines the curvature of the target space and the inflaton field  $\phi^I$  as in Eq. (26). This observable  $r$  has not yet been determined, but the bounds of the amplitude of the gravitational perturbations have dramatically improved since COBE, and further experiments to constrain  $r$  are currently under construction. The main point of these efforts of course is to detect primordial gravitational waves and in the process determine some of the characteristic features of inflation. However, while the scale of inflation is an important characteristic, it is not the only information tied to  $r$ , and even in the absence of a detection, the results of future experiments are important because they provide essential constraints for inflationary model building. While an improvement of an order of magnitude in the recent past has not provided insight into the scale of inflation [65], the experimental achievements have been strong enough to exclude an infinite number of models, among them the class of monomial inflation potentials.

### A. Large field inflation and small tensor-to-scalar ratios

One of the issues in which the bounds on  $r$  have been instrumental is the question whether the experimental target values predicted to be reached in the near future will

be able to exclude certain types of inflationary models. As noted above, this has already been achieved by the exclusion of certain sequences of models. A more far reaching discussion that has been conducted in a large number of papers, following [65], is concerned with the question of whether there are bounds that can exclude large field inflation altogether. In the past, strong bounds have been suggested based on restricting consideration to special classes of inflationary models, and some of these bounds have been used in proposals for new observatories. It was, in particular, noted early on that a nondetection of  $r$  at the level of  $10^{-2}$  [86] or  $10^{-3}$  [87] would rule out large field inflation, see also [88]. This value was subsequently reduced somewhat, depending on specific assumptions made in the analysis. Slightly lower constraints than the milli-scale mentioned above were obtained in [89,90] in the context of single field inflation. For a special class of models, this bound was pushed down further in [91], where it was argued that large field inflation is only possible if this ratio is larger than  $r \geq 2 \times 10^{-5}$ . In light of these discussions, it is of interest to analyze the tensor-to-scalar ratio  $r$  in the more general context of multifield inflation with curved target spaces.

The current experimental bound for  $r$  is several magnitudes above the most stringent values just quoted. An often cited value is the result reported by the PLANCK experiment, which is reported to be given by  $r \leq 0.06$  [1,2]. Such bounds depend on the type of fit adopted in the experimental analysis, and the above value was obtained by assuming a minimal number of parameters, which is not appropriate for multifield inflation. Extensions beyond the standard six parameter fits have been considered, but at present, no PLANCK based full analysis appropriate for two field inflation is available in the literature. In the following, the single field bound will be therefore adopted as the constraint. Ongoing experiments such as CLASS [6,92] aim to reduce the PLANCK bound to the level of  $10^{-2}$ , while upcoming and future ground based experiments such as the Simons Observatory, the BICEP Array, and the CMB-S4 project will be able to reduce this by more than an order of magnitude [4,5,93–96]. The satellite experiment Light BIRD [97] is designed to reach down to  $r = 2 \times 10^{-3}$  at 95% C.L., while the target value of the proposed satellite experiment PICO [98,99] reaches further down by almost another order of magnitude to  $r = 5 \times 10^{-4}$  at a  $5\sigma$  confidence level, with  $\sigma(r) = 1 \times 10^{-4}$  at  $r = 0$ . As noted already, even a nondetection of the tensor modes at this level would have significant effects on the current inflationary model landscape, and it would provide a better perspective on different *ad hoc* selection rules that have been used to provide a lower bound on  $r$  [100].

The goal in the present section is to analyze the tensor-to-scalar ratio of  $j$ -inflation in light of the experimental and theoretical bounds discussed above. The systematic

results are of course limited by the resolution of the scans, but even so, it becomes clear from the analysis below that the parameter space of  $j$ -inflation is constrained by the PLANCK bounds on  $r$ ; hence,  $j$ -inflation presents a target for upcoming and planned experiments. It also becomes clear that there are regions in parameter space in which the lower bound of  $r$  can be pushed below the experimental floor of all upcoming experiments. The  $r$  range of  $j$ -inflation, in particular, reaches below the boundary that has been identified in the literature as the dividing line for large field inflation in the single field context. The fact that  $j$ -inflation can reach below these proposed large field boundaries alleviates the concerns expressed in a number of recent discussions [94,95,98,99,101] that the measurement of an experimental bound for the tensor ratio below  $r \cong 10^{-3}$  would force a significant change in our understanding of the primordial Universe. The example of  $j$ -inflation shows that the framework of two field inflation is able to reach below these thresholds.

## B. Global $r$ -scan

As in all scans of the target space, the specific results obtained for the tensor ratio depend on the size of the fundamental lattice cell as well as the parameter  $\mu$  that is not fixed by the CMB amplitude in the formulation considered here. What does not change is the global structure of the results. As in the case of the spectral index, it is useful to consider the shape of the analytical form of the tensor ratio  $r(\tau^l)$  of  $j$ -inflation as a function on the target space via Eq. (26). This is shown in Fig. 11.

In Fig. 12, the results are given for a global scan of  $r$  along the central vertical band. The resulting pattern of this band is repeated in the upper half plane to the left and right by the shift symmetry  $\tau \rightarrow \tau + 1$  that is part of the modular group  $SL(2, \mathbb{Z})$  that leaves the potential invariant. It is this invariance that is part of the motivation of modular and, more generally, automorphic inflation [7,8]. The structure of the central band changes in dependence of the distance to the real axis. The areas closer to the boundary of the target space given by  $\text{Im}\tau = 0$  are distorted in the plot of Fig. 12 because it is drawn by using the euclidean metric. The hyperbolic metric that describes the actual geometry of the field space increasingly stretches these domains as the horizontal boundary is approached because of the factor  $1/(\text{Im}\tau)^2$  that enters  $ds^2$ . This measure leads to finite volumes of the target space in which the PLANCK bound on the tensor ratio is satisfied.

## C. Effect of the field space curvature $R_{fs}$ on the tensor ratio $r$

Recall from the discussion above that once the energy scale  $\mu$  is chosen the overall scale  $\Lambda$  of the potential follows from the CMB amplitude, making  $\mu$  the only parameter that can be varied. This means that the only free parameter in the

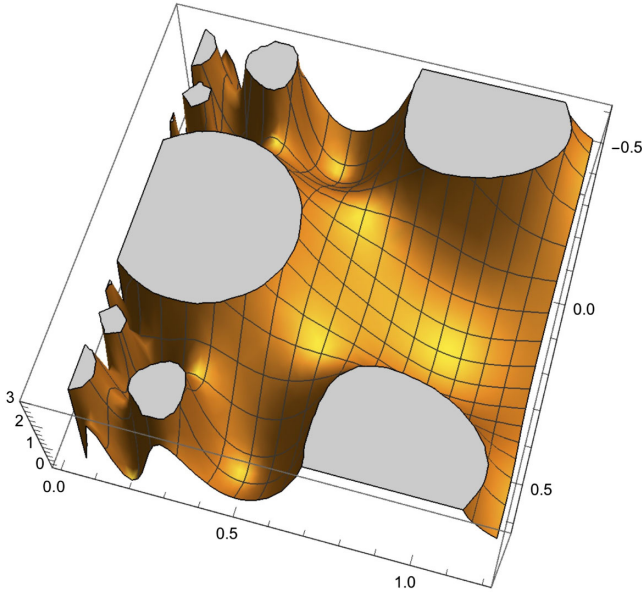


FIG. 11. A global 3D graph of the tensor-to-scalar ratio  $r(\tau^I)$  along the vertical axis on the field space  $(\tau^1, \tau^2)$  in the fundamental band. This illustrates the behavior of  $r(\tau^I)$  in Eq. (26).

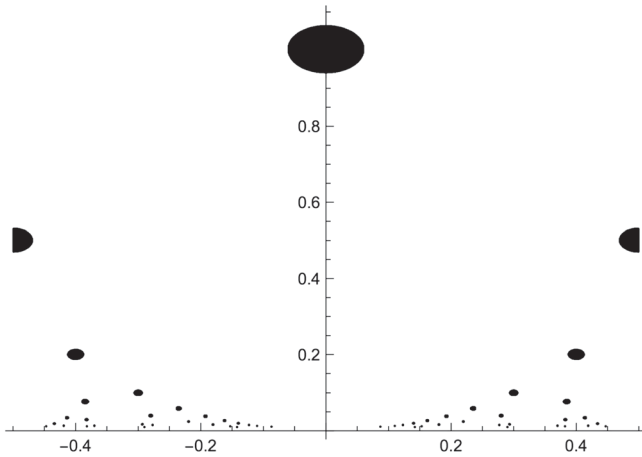


FIG. 12. Results from a global scan for viable initial values in the  $(\tau^1, \tau^2)$  field space along the central fundamental band that are consistent with the tensor ratio bound. Close to the horizontal axis, the effect of the hyperbolic metric leads to a stretching of the Euclidean distances of this plot.

model is the curvature scalar of the target space  $R_{\text{fs}} = -2/\mu^2$  determined by the metric, Eq. (12). The tensor ratio in Eq. (26) shows that  $r$  scales like  $1/\mu^2$ ; hence, it scales with the scalar curvature  $R_{\text{fs}}$  of the field space

$$r = -64\pi^2 M_{\text{Pl}}^2 R_{\text{fs}} (\text{Im}\tau)^2 \left| \frac{E_6}{E_4} \right|^2. \quad (44)$$

The second ingredient that varies is the inflaton value  $\phi_*^I$  at horizon crossing, and these two parameters determine the range of  $r$ . The precise boundary values of  $\mu$ , or  $R_{\text{fs}}$ , and  $\phi_*^I$

depend on the range of the number of  $e$ -folds and on the lattice resolution of the scan.

To be concrete, for a fixed value of the target space curvature  $R_{\text{fs}}$  via a choice of  $\mu$  the initial values  $\tau_*^I$  that satisfy the constraints adopted for  $r, n_{\mathcal{R}\mathcal{R}}$  and  $N_*$  sweep out a finite band in the  $(n_{\mathcal{R}\mathcal{R}}, r)$  plane. As the target space curvature is varied, this band moves up and down along the axis defined by the tensor ratio  $r$ . It is *a priori* not transparent how the imposed constraints combine to determine the specific boundaries and the band in the  $(n_{\mathcal{R}\mathcal{R}}, r)$  plane. This is illuminated by considering a three-dimensional plot which adds the number of  $e$ -folds  $N_*$  to this plane. Figure 13 shows that doing so explains the boundaries as determined by the bounds adopted for  $N_*$ . This lifting of the planar plot shows that the lower bound on  $r$  arises from the upper bound of the number of  $e$ -folds. If the upper limit  $N_*$  would be increased, the lower bound on  $r$  would decrease for fixed  $\mu$ . The degeneracy of the sheet in Fig. 13 along the direction of the spectral index shows that in  $j$ -inflation a scaling relation exists between the tensor ratio  $r_*$  and the number of  $e$ -folds  $N_*$ . Parametrizing the tensor ratio as  $r = \alpha N^{-\beta}$ , one obtains for  $\beta = 1$  the monomial class, for  $\beta = 2$  the Starobinsky type range of  $r$ , and for higher  $\beta$  the range covered by  $j$ -inflation, with increasing suppression obtained for larger target space curvature  $R_{\text{fs}}$ .

The issue of the upper limit for  $N_*$  has a long history, and the specific bound  $N_* \leq 70$ , while often adopted, is not sharp. Discussions of the allowed range of the number of  $e$ -folds during inflation can be found in [102,103], and their implications for trans-Planckian physics have also been extensively discussed. A review of these issues can be found in [67].

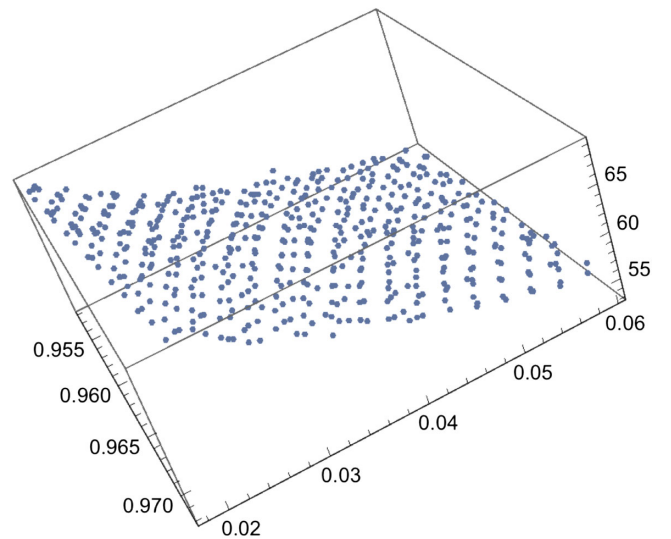


FIG. 13. The  $N_*$  dependence in the  $(n_{\mathcal{R}\mathcal{R}}, r, N_*)$  space at fixed  $\mu$ : as the number of  $e$ -folds grow the tensor ratio  $r$  decreases. The initial values here are required to satisfy the constraints imposed on the spectral index  $n_{\mathcal{R}\mathcal{R}}$ , the tensor ratio  $r$ , and the number of  $e$ -folds  $N_* \in [50, 70]$ .

As noted above, the band swept out in the plane spanned by  $n_{\mathcal{R}\mathcal{R}}$  and  $r$  in dependence of the CMB constraint on the spectral index and the adopted range for the number of  $e$ -folds depend on the energy scale  $\mu$  that determines the field space curvature  $R_{\text{fs}}$ . As the bounds obtained by the PLANCK probe will be improved by the next generation of experiments currently under construction, the bound on the curvature scalar will become stronger. This raises the question of how much the tensor ratio is affected by a variation of the target space curvature that remains consistent with the PLANCK bounds on the spectral index and  $N_*$ . In Fig. 14, the results for  $R_{\text{fs}} = 1/\mu^2$  with  $\mu = 27M_{\text{Pl}}$  and  $\mu = 35M_{\text{Pl}}$  are shown. This graph illustrates that the  $r$  bands determined by the target space curvature lie for both energy scales  $\mu$  within the confidence region of the PLANCK results. As the curvature  $R_{\text{fs}}$  increases, the band moves lower into the region targeted by the Simons Observatory [94]. This shows that the range of the tensor ratio obtained in  $j$ -inflation for different  $\mu$  contains and extends the region of the  $r$  value obtained within the class of monomial inflation, as well as that of the Starobinsky model [84]. The latter, in particular, is a prominent model that has motivated some experimental proposals in the recent past.

The analysis of this section shows that  $j$ -inflation provides an interesting target for experiments that aim to discover the gravitational contribution of the CMB signal, or at least to significantly improve the constraints on the

tensor ratio. This includes experiments that are scheduled to come online in the near future, such as the Simons Observatory, CMB-S4, as well as the satellite experiment LightBird. The results from these observations will have an impact on the size of the field space curvature of the hyperbolic field space of modular inflation.

## XI. EFFECTS OF $\mu$ VARIATIONS

Modular inflation as described in Sec. III is parametrized by the energy scale  $\Lambda$  and the inflaton scale  $\mu$  needed to make the inflaton dimensionless. The scale  $\Lambda$  of the potential is as usual determined by the amplitude of the CMB power spectrum measured by the satellite experiments. This leaves the scale  $\mu$  as an *a priori* undetermined parameter of the theory, which is related to the field space scalar curvature via Eq. (12). This parameter is constrained however by the CMB results for the observables, such as the spectral index and the bound on the tensor ratio. Any scan of the target space is of course limited by the adopted lattice resolution and other run parameters that are constrained by CPU resources. The scans discussed were mostly performed with a fixed  $\mu$ , and the question arises of how these change when  $\mu$  is varied. This is illustrated for the spectral constraint  $n_{\mathcal{R}\mathcal{R}}$  in Fig. 15, which represents a compilation of initial inflaton values that satisfy the PLANCK constraint for the range of  $\mu \in [25, 50]M_{\text{Pl}}$ . The modular symmetry of the  $j$ -inflation model implies that the same structure is repeated along the modular sequences described in Secs. IV and V, repeating this pattern indefinitely.

Imposing not only the spectral index but also the tensor-ratio bound of PLANCK and the constraint on the number of  $e$ -folds  $N_*$  selects from the distribution of Fig. 15 a subset of initial values that for the same range of  $\mu$  values and the same run parameters produces a region in the target space of the form of a nutcracker, shown in Fig. 16.

A natural question that can next be raised is how the tensor-to-scalar ratio  $r$  behaves as the energy scale is varied. In the context of the  $(n_{\mathcal{R}\mathcal{R}}, r)$  plane usually considered by the CMB collaborations, this has been discussed in Sec. X and illustrated in Fig. 14. In Fig. 17, this is addressed by considering the 3D distribution of the parameters  $(n_{\mathcal{R}\mathcal{R}}, r, N_*)$  for three different values of  $\mu$ . This plot allows one to extrapolate the structure for the intermediate values and also allows to infer how the pattern extends beyond the values shown. The different bands in dependence of  $\mu$  show that the scaling relation mentioned in the previous section between  $r_*$  and  $N_*$  varies with  $\mu$ .

## XII. CONCLUSIONS

The present paper has conducted an extensive systematic analysis of the inflaton behavior in modular inflation with the potential given by the  $j$  function. In the process, it has become apparent that the field space has an interesting structure that originates from the underlying symmetry,

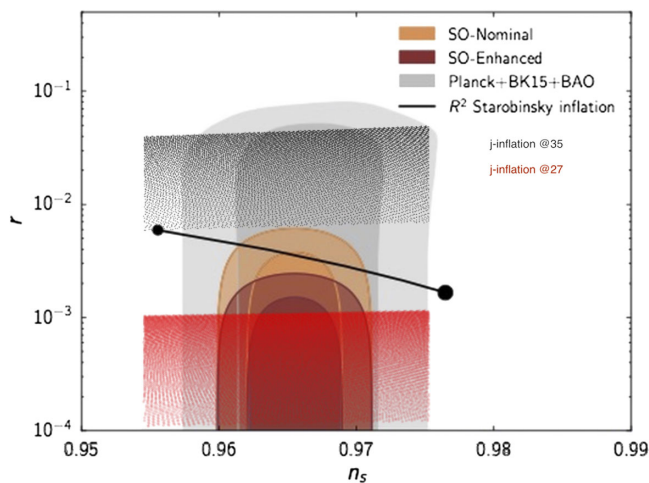


FIG. 14. The results obtained for two scans of  $j$ -inflation at energy scales  $\mu/M_{\text{Pl}} = 27, 35$ , with associated curvature  $R_{\text{fs}}$  of the target space, projected onto the Simons Observatory confidence regions [94]. Here, the number of  $e$ -folds for all points satisfies the constraint  $N_* \in [50, 70]$ . The results for the larger  $\mu$  value (upper band of black points) intersect with the PLANCK range but not with the target range of the Simons telescope. For the smaller  $\mu$  value (lower band of red points), the distribution intersects with the region described by the Simons Array Collaboration.

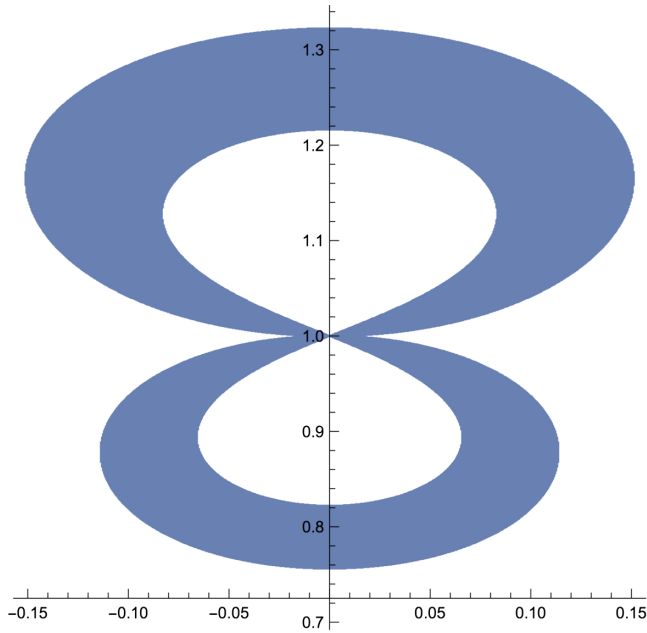


FIG. 15. A compilation of results in the dimensionless field space  $(\tau^1, \tau^2)$  for the spectral scalar index for  $\mu/M_{\text{Pl}}$  variations between 25 and 50 in the region around the saddle point  $\tau_s = i$ .

which allows one to perform a quite complete scan of the total target space, due in part to the shift symmetry that defines an element of the modular invariance. The shift symmetry, in particular, makes it possible to effectively scan completely the part of the target space constrained by the PLANCK data because it leads to a decomposition of the target space into an infinite number of vertical bands that all have the same field theoretic behavior. Within each of these bands, the tessellation induced by the modular invariance in turn leads to an iterative structure that maps large field regions to regions where the initial field components take values that are arbitrarily small. This shows that modular invariant inflation is a framework in which the distinction between large field and small field inflation into separate classes no longer holds. As a result, the notion of large field and small field inflation is not a model characteristic of general inflationary models. While this has been shown here in the context of a particular model, the modularity admitted by this type of geometry generalizes to other models in this class of theories. In the more general context of automorphic inflation with an arbitrary number of inflaton components, a similar symmetry structure arises where the modular groups are replaced by discrete groups  $G(\mathbb{Z})$  for reductive groups  $G(\mathbb{R})$  [7,8]. As a result, the classification of inflation should, in general, proceed along lines that do not reference the dichotomy of large field vs. small field inflation. A further implication of the tessellation of the field space in combination with the structure of the  $j$ -inflation potential is that in the geometric measure provided by the target space metric the fraction of the volume of the field space that leads to sufficient inflation is finite.

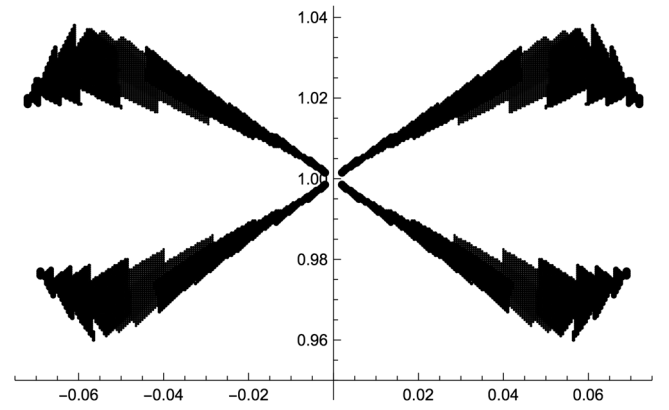


FIG. 16. The nutcracker in the  $(\tau^1, \tau^2)$  plane obtained from the constraints  $n_{\mathcal{RR}} \cap r \cap N_*$  for the runs in the previous graph, i.e.,  $\mu/M_{\text{Pl}} \in [25, 50]$ .

A characteristic feature of the potential surface of  $j$ -inflation is a wall-like structure of the potential along the vertical direction of the inflaton doublet. The motion of the inflaton along this wall is of geodesic type and is restricted by the phenomenological constraints. Trajectories that are compatible with the PLANCK data exist in neighborhoods around the critical points of the potential, leading to inflaton orbits that, in general, are different from hyperbolic geodesics but can approximate them as the initial values get closer to these critical points. As a result, while the presence of the hyperbolic metric in modular inflation has important implications for the structure of the theory, the dynamics determined by the potential is crucial for the behavior of the

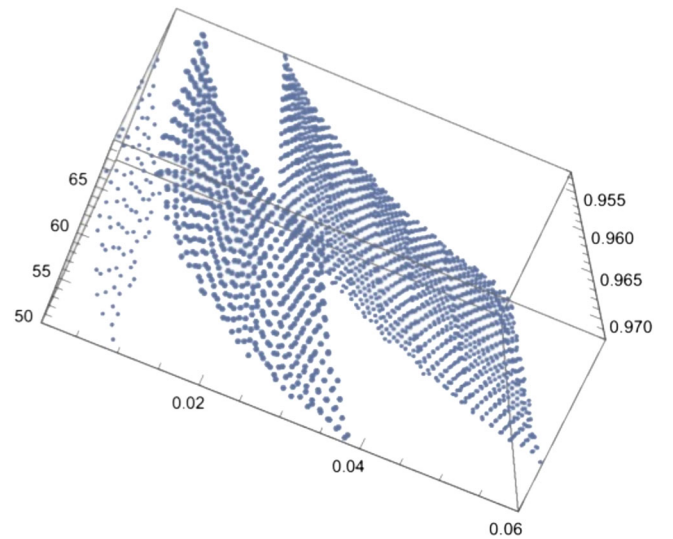


FIG. 17. Illustration of the  $\mu$  dependence of the  $(n_{\mathcal{RR}}, r, N_*)$  distribution for  $\mu \in \{30, 35, 40\}$ . Here,  $N_*$  is along the vertical axis, and  $(n_{\mathcal{RR}}, r)$  defines the lower plane. This graph shows how the distribution shown in Fig. 13 for a fixed  $\mu$  moves from the right to the left with decreasing  $\mu$  and that the degeneracy of the distributions along the direction of the spectral index is independent of the choice of  $\mu$ .

inflaton. In particular, the attractor structure of the model is determined by the potential, as expected. Nevertheless, there are regions in the target space where the geometry of the inflaton trajectories follows closely that of the different types of geodesics that characterize the upper half plane hyperbolic target space. In the context of the dynamical structure, the attractors in the potential surface project down to trajectories that are close to the two different types of geodesics that are encountered in hyperbolic geometry.

The phenomenological part of the analysis first shows that the region of the target space with sufficient inflation in the canonical range has the shape of a butterfly that covers a finite fraction the total field space. Imposing further the CMB constraints on the spectral index and the tensor ratio leads to initial values for which the spectral index admits an approximate scaling behavior that is reminiscent of the scaling behavior of monomial and Starobinsky inflation. Nevertheless the bounds on  $r$  that have been discussed in the literature in the context of single field inflation are not satisfied in  $j$ -inflation. A detailed analysis of the tensor ratio on the space of initial values instead shows that upcoming gravity wave experiments that can reach down to  $r \simeq 10^{-4}$  and even smaller will not be able to distinguish

between large and small field inflation. These experiments are nevertheless important even in the absence of a discovery because they provide essential constraints for model building. They will, in particular, constrain the parameter space for  $j$ -inflation, which presents a prime target for future observations.

The CMB constraints that have been obtained since COBE have established the amplitude of the scalar power spectrum, leading to a normalization of the overall energy scale of inflationary models. In  $j$ -inflation as described in the present paper, this leaves the second energy parameter  $\mu$ , which is constrained by the phenomenological parameters just discussed. This energy scale uniquely determines the curvature scalar of the field space; hence, these observational constraints put bounds on how strongly curved this target space can be.

### ACKNOWLEDGMENTS

It is a pleasure to thank Monika Lynker and Deepu Sengupta for discussions. This work was supported by a sabbatical leave of absence from Indiana University South Bend.

- 
- [1] N. Aghanim *et al.* (PLANCK Collaboration), Planck 2018 results. VI. Cosmological parameters, *Astron. Astrophys.* **641**, A6 (2020).
  - [2] Y. Akrami *et al.* (PLANCK Collaboration), Planck 2018 results. X. Constraints on inflation, *Astron. Astrophys.* **641**, A10 (2020).
  - [3] P. A. R. Ade *et al.*, BICEP2/Keck Array X: Constraints on Primordial Gravitational Waves using Planck, WMAP, and New BICEP2/Keck Observations through the 2015 Season, *Phys. Rev. Lett.* **121**, 221301 (2018).
  - [4] P. Ade *et al.*, The Simons Observatory: Science goals and forecasts, *J. Cosmol. Astropart. Phys.* **02** (2019) 056.
  - [5] K. N. Abazajian *et al.*, CMB-S4 science case, reference design, and project plan, [arXiv:1907.04473](https://arxiv.org/abs/1907.04473).
  - [6] S. Dahal *et al.* (CLASS Collaboration), Four-year cosmology large angular scale surveyor (CLASS) observations: On-sky receiver performance at 40, 90, 150 and 220 GHz frequency bands, *Astrophys. J.* **926**, 33 (2022).
  - [7] R. Schimmrigk, Automorphic inflation, *Phys. Lett. B* **748**, 376 (2015).
  - [8] R. Schimmrigk, A general framework of automorphic inflation, *J. High Energy Phys.* **05** (2016) 140.
  - [9] R. Schimmrigk, Modular inflation observables and  $j$ -inflation phenomenology, *J. High Energy Phys.* **09** (2017) 043.
  - [10] R. Schimmrigk, Multifield reheating after modular  $j$ -inflation, *Phys. Lett. B* **782**, 193 (2018).
  - [11] M. Lynker and R. Schimmrigk, Modular inflation at higher level  $N$ , *J. Cosmol. Astropart. Phys.* **06** (2019) 036.
  - [12] J. J. M. Carrasco, R. Kallosh, and A. Linde, Hyperbolic geometry and cosmological attractors, *Phys. Rev. D* **92**, 04130 (2015).
  - [13] J. J. M. Carrasco, R. Kallosh, and A. Linde, Cosmological attractors and initial conditions for inflation, *Phys. Rev. D* **92**, 063519 (2015).
  - [14] V. Aragam, S. Paban, and R. Rosati, Multi-field inflation in high-slope potentials, *J. Cosmol. Astropart. Phys.* **04** (2020) 022.
  - [15] A. Achucarro and Y. Welling, Orbital inflation: Inflating along an angular isometry of field space, [arXiv:1907.02020](https://arxiv.org/abs/1907.02020).
  - [16] R. Kallosh and A. Linde, Multi-field conformal cosmological attractors, *J. Cosmol. Astropart. Phys.* **12** (2013) 006.
  - [17] R. Kallosh, A. Linde, and D. Roest, Large field inflation and double  $\alpha$ -attractors, *J. High Energy Phys.* **08** (2014) 052.
  - [18] R. Kallosh and A. Linde, Escher in the sky, *Comput. Rend. Phys.* **16** (2015) 914.
  - [19] A. Achucarro, R. Kallosh, A. Linde, D.-G. Wang, and Y. Welling, Universality of multi-field  $\alpha$ -attractors, *J. Cosmol. Astropart. Phys.* **04** (2018) 028.
  - [20] A. Brown, Hyperbolic Inflation, *Phys. Rev. Lett.* **121**, 251601 (2018).
  - [21] C. I. Lazaroiu and C. S. Shahbazi, Generalized two-field  $\alpha$ -attractor models from geometrically finite hyperbolic surfaces, *Nucl. Phys.* **B936**, 542 (2018).

- [22] E. M. Babalic and C. I. Lazaroiu, Generalized  $\alpha$ -attractors from the hyperbolic triply-punctured sphere, *Nucl. Phys.* **B937**, 434 (2018).
- [23] S. Mizuno and S. Mukohyama, Primordial perturbations from inflation with a hyperbolic field-space, *Phys. Rev. D* **96**, 103533 (2017).
- [24] A. Linde, D.-G. Wang, Y. Welling, and A. Achúcarro, Hypernatural inflation, *J. Cosmol. Astropart. Phys.* **07** (2018) 035.
- [25] L. Anguelova, E. M. Babalic, and C. I. Lazaroiu, Hidden symmetries of two-field cosmological models, *J. High Energy Phys.* **09** (2019) 007.
- [26] S. Mizuno, S. Mukohyama, S. Pi, and Y.-L. Zhang, Hyperbolic field space and swampland conjecture for DBI scalar, *J. Cosmol. Astropart. Phys.* **09** (2019) 072.
- [27] M. Bounakis, I. G. Moss, and G. Rigoropoulos, Observational constraints on hyperinflation, *J. Cosmol. Astropart. Phys.* **02** (2021) 006.
- [28] V. Aragam, S. Paban, and R. Rosati, The multi-field, rapid-turn inflationary solution, *J. High Energy Phys.* **03** (2021) 009.
- [29] X. Chen, G. A. Palma, W. Riquelme, B. S. Hitschfeld, and S. Sypsas, Landscape tomography through primordial non-Gaussianity, *Phys. Rev. D* **98**, 083528 (2018).
- [30] T. Bjorkmo and M. C. D. Marsh, Hyperinflation generalised: From its attractor mechanism to its tension with the ‘swampland conditions’, *J. High Energy Phys.* **04** (2019) 172.
- [31] P. Christodoulidis, D. Roest, and E. I. Sfakianakis, Attractors, bifurcations and curvature in multi-field inflation, *J. Cosmol. Astropart. Phys.* **08** (2020) 006.
- [32] O. Grocholski, M. Kalinowski, M. Kolanowski, S. Renaux-Petel, K. Turzynski, and V. Vennin, On backreaction effects in geometrical destabilisation of inflation, *J. Cosmol. Astropart. Phys.* **05** (2019) 008.
- [33] D.-G. Wang, On the inflationary massive field with a curved field manifold, *J. Cosmol. Astropart. Phys.* **01** (2020) 046.
- [34] R. Kallosh and A. Linde, CMB targets after Planck, *Phys. Rev. D* **100**, 123523 (2019).
- [35] R. Bravo, G. A. Palma, and S. Riquelme, A tip for landscape riders: Multi-field inflation can fulfill the swampland distance conjecture, *J. Cosmol. Astropart. Phys.* **02** (2020) 004.
- [36] A. Linde, Hybrid inflation, *Phys. Rev. D* **49**, 748 (1994).
- [37] G. Lazarides, C. Panagiotakopoulos, and N. D. Vlachos, Initial conditions for smooth hybrid inflation, *Phys. Rev. D* **54**, 1369 (1996).
- [38] G. Lazarides and N. D. Vlachos, Initial conditions for supersymmetric inflation, *Phys. Rev. D* **56**, 4562 (1997).
- [39] N. Tetradis, Fine tuning of the initial conditions for hybrid inflation, *Phys. Rev. D* **57**, 5997 (1998).
- [40] L. E. Mendes and A. R. Liddle, Initial conditions for hybrid inflation, *Phys. Rev. D* **62**, 103511 (2000).
- [41] S. Clesse and J. Rocher, Avoiding the blue spectrum and the fine-tuning of initial conditions in hybrid inflation, *Phys. Rev. D* **79**, 103507 (2009).
- [42] S. Clesse, C. Ringeval, and J. Rocher, Fractal initial conditions and natural parameter values in hybrid inflation, *Phys. Rev. D* **80**, 123534 (2009).
- [43] S. Clesse, Hybrid inflation along waterfall trajectories, *Phys. Rev. D* **83**, 063518 (2011).
- [44] R. Easter and L. C. Price, Initial conditions and sampling for multifield inflation, *J. Cosmol. Astropart. Phys.* **07** (2013) 027.
- [45] S. Clesse and J. Rekier, Updated constraints on large field hybrid inflation, *Phys. Rev. D* **90**, 083527 (2014).
- [46] P. Carrilho, D. Mulryne, J. Ronayne, and T. Tenkanen, Attractor behavior in multifield inflation, *J. Cosmol. Astropart. Phys.* **06** (2018) 032.
- [47] G. Gibbons, S. Hawking, and J. Stewart, A natural measure on the set of all universes, *Nucl. Phys.* **B281**, 736 (1987).
- [48] S. Hawking and D. N. Page, How probable is inflation?, *Nucl. Phys.* **298**, 789 (1988).
- [49] G. Gibbons and N. Turok, The measure problem in cosmology, *Phys. Rev. D* **77**, 063516 (2008).
- [50] S. M. Carroll and H. Tam, Unitary evolution and cosmological fine-tuning, [arXiv:1007.1417](https://arxiv.org/abs/1007.1417).
- [51] J. S. Schiffrin and R. M. Wald, Measure and probability in cosmology, *Phys. Rev. D* **86**, 023521 (2012).
- [52] G. N. Remmen and S. M. Carroll, Attractor solutions in scalar-field cosmology, *Phys. Rev. D* **88**, 083518 (2013).
- [53] V. Mukhanov, Quantum cosmological perturbations: Predictions and observations, *Eur. Phys. J. C* **73**, 2486 (2013).
- [54] D. Roest, Universality classes of inflation, *J. Cosmol. Astropart. Phys.* **01** (2014) 007.
- [55] P. Creminelli, S. Dubovsky, D. Lopez Nacir, M. Simonovic, G. Trevisan, G. Villadoro, and M. Zaldarriaga, Implications of the scalar tilt for the tensor-to-scalar ratio, *Phys. Rev. D* **92**, 123528 (2015).
- [56] V. N. Lukash, Production of sound waves in the early universe, *Zh. Eksp. Teor. Fiz.* **31**, 631 (1980).
- [57] J. M. Bardeen, Gauge-invariant cosmological perturbations, *Phys. Rev. D* **22**, 1882 (1980).
- [58] S. Weinberg, *Cosmology* (Cambridge University Press, Cambridge, England, 2008).
- [59] R. Krishnan, Symmetries of stationary points of the  $G$ -invariant potential and the framework of the auxiliary group, *Phys. Rev. D* **103**, L051701 (2021).
- [60] S. Dodelson, W. H. Kinney, and E. W. Kolb, Cosmic microwave background measurements can discriminate among inflation models, *Phys. Rev. D* **56**, 3207 (1997).
- [61] W. H. Kinney, Constraining inflation with CMB polarization, *Phys. Rev. D* **58**, 123506 (1998).
- [62] S. Hannestad, S. H. Hansen, and F. L. Villante, Probing the power spectrum bend with recent CMB data, *Astropart. Phys.* **16**, 137 (2001).
- [63] H. V. Peiris *et al.* (WMAP Collaboration), First year WMAP observations: Implications for inflation, *Astrophys. J. Suppl. Ser.* **148**, 213 (2003).
- [64] W. H. Kinney, E. W. Kolb, A. Melchiorri, and A. Riotto, WMAPping inflationary physics, *Phys. Rev. D* **69**, 103516 (2004).
- [65] D. H. Lyth, What Would We Learn by Detecting a Gravitational Wave Signal in the Cosmic Microwave Background Anisotropy?, *Phys. Rev. Lett.* **78**, 1861 (1997).
- [66] J. Milnor, On the concept of attractors, *Commun. Math. Phys.* **99**, 177 (1985).

- [67] R. Brandenberger, Initial conditions for inflation – a short review, *Int. J. Mod. Phys.* **26**, 1740002 (2016).
- [68] A. Linde, On the problem of initial conditions for inflation, *Found. Phys.* **48**, 1246 (2018).
- [69] K. Finn and S. Karamitsos, Finite measure for the initial conditions of inflation, *Phys. Rev. D* **99**, 063515 (2019); **99**, 109901(E) (2019).
- [70] E. Palti, The swampland: Introduction and review, *Fortschr. Phys.* **67**, 1900037 (2019).
- [71] Z. Wang, R. Brandenberger, and L. Heisenberg, Eternal inflation, entropy bounds and swampland, *Eur. Phys. J. C* **80**, 864 (2020).
- [72] H. Ooguri and C. Vafa, On the geometry of the string landscape and the swampland, *Nucl. Phys.* **766**, 21 (2007).
- [73] R. Schimmrigk, The swampland spectrum conjecture in inflation, [arXiv:1810.11699](https://arxiv.org/abs/1810.11699).
- [74] C. Vafa, The string landscape and the swampland, [arXiv:hep-th/0509212](https://arxiv.org/abs/hep-th/0509212).
- [75] M. R. Douglas and Z. Lu, Finiteness of volume of moduli spaces, [arXiv:hep-th/0509224](https://arxiv.org/abs/hep-th/0509224).
- [76] G. Obied, H. Ooguri, L. Spodyneiko, and C. Vafa, de Sitter and the swampland, [arXiv:1806.08362](https://arxiv.org/abs/1806.08362).
- [77] A. Bedroya and C. Vafa, Trans-Planckian censorship and the swampland, *J. High Energy Phys.* **09** (2020) 123.
- [78] A. Bedroya, R. Brandenberger, M. Loverde, and C. Vafa, Trans-Planckian censorship and inflationary cosmology, *Phys. Rev. D* **101**, 103502 (2020).
- [79] G. Dvali, A. Kehagias, and A. Riotto, Inflation and decoupling, [arXiv:2005.05146](https://arxiv.org/abs/2005.05146).
- [80] C. P. Burgess, S. P. de Alwis, and F. Quevedo, Cosmological Trans-Planckian conjectures are not effective, *J. Cosmol. Astropart. Phys.* **05** (2021) 037.
- [81] R. Brandenberger, Trans-Planckian censorship conjecture and early universe cosmology, *Lett. High Energy Phys.* **198** (2021).
- [82] E. Di Valentino, A. Mechiorri, and J. Silk, Cosmological constraints in extended parameter space from the PLANCK 2018 legacy release, *J. Cosmol. Astropart. Phys.* **01** (2020) 013.
- [83] M. S. Turner, Coherent scalar-field oscillations in an expanding universe, *Phys. Rev. D* **28**, 1243 (1983).
- [84] A. A. Starobinsky, A new type of isotropic cosmological models without singularity, *Phys. Lett.* **91B**, 99 (1980).
- [85] G. Hinshaw *et al.* (WMAP Collaboration), Nine-year WMAP observations: Cosmological parameter results, *Astrophys. J. Suppl. Ser.* **208**, 19 (2013).
- [86] D. Baumann *et al.* (CMBPol Study Team), CMBPol Mission concept study: A mission to map our origins, *AIP Conf. Proc.* **1141**, 10 (2009).
- [87] K. N. Abazajian *et al.*, Inflation physics from the CMB and large scale structure, *Astropart. Phys.* **63**, 55 (2015).
- [88] G. Efstathiou and S. Chongchitnan, The search for primordial tensor modes, *Prog. Theor. Phys. Suppl.* **163**, 204 (2006).
- [89] J. Garcia-Bellido, D. Roest, M. Scalisi, and I. Zavala, The Lyth bound of inflation with a tilt, *Phys. Rev. D* **90**, 123539 (2014).
- [90] Q.-G. Huang, Lyth bound revisited, *Phys. Rev. D* **91**, 123532 (2015).
- [91] A. Linde, Gravitational waves and large field inflation, *J. Cosmol. Astropart. Phys.* **02** (2017) 006.
- [92] J. Iuliano *et al.*, The cosmology large angular scale surveyor receiver design, *Proc. SPIE Int. Soc. Opt. Eng.* **10708**, 1070828 (2018).
- [93] H. Hui *et al.*, BICEP Array: A multi-frequency degree-scale CMB polarimeter, in *Millimeter, Submillimeter, and Far-Infrared Detectors and Instrumentation for Astronomy IX*, ser. Society of Photo-Optical Instrumentation Engineers (SPIE) Conference Series Vol. 10708 (2018), p. 1070807.
- [94] M. H. Abitbol *et al.*, The Simons Observatory, Astro2020 APC Decadal Project White Paper, *Bull. Am. Astron. Soc.* **51**, 147 (2019).
- [95] K. N. Abazajian *et al.*, CMB-S4 Decadal survey APC white paper, *Bull. Am. Astron. Soc.* **51**, 209 (2019).
- [96] K. N. Abazajian *et al.*, CMB-S4: Forecasting constraints on primordial gravitational waves, [arXiv:2008.12619](https://arxiv.org/abs/2008.12619).
- [97] M. Hazumi *et al.* (LiteBIRD Collaboration), LiteBIRD: A satellite for the studies of B-mode polarization from cosmic background detection, *J. Low Temp. Phys.* **194**, 443 (2019).
- [98] S. Hanany *et al.*, PICO: Probe of inflation and cosmic origins, [arXiv:1902.10541](https://arxiv.org/abs/1902.10541).
- [99] M. Alvarez *et al.*, PICO: Probe of inflation and cosmic origins, [arXiv:1908.07495](https://arxiv.org/abs/1908.07495).
- [100] L. Boyle, P. Steinhardt, and N. Turok, Inflationary Predictions for Scalar and Tensor Fluctuations Reconsidered, *Phys. Rev. Lett.* **96**, 111301 (2006).
- [101] S. Shandera *et al.*, Probing the origin of our universe through cosmic microwave background constraints on gravitational waves, *Bull. Am. Astron. Soc.* **51**, 338 (2019).
- [102] S. Dodelson and L. Hui, Horizon Ratio Bound for Inflationary Fluctuations, *Phys. Rev. Lett.* **91**, 131301 (2003).
- [103] A. R. Liddle and S. M. Leach, How long before the end of inflation were observable perturbations produced?, *Phys. Rev. D* **68**, 103503 (2003).